Technical Report
1213

Undersea Laser Communications Field Test at the Naval Undersea Warfare Center (NUWC)

A.S. Fletcher
H.G. Rao
N.D. Hardy
C.E. DeVoe
I.D. Gaschits
F. Hakimi
S.A. Hamilton
R.D. Kaminsky
M.S. Scheinbart
T.M. Yarnall
J.G. Ingwersen

30 August 2016

Lincoln Laboratory
MASSACHUSETTS INSTITUTE OF TECHNOLOGY
LEXINGTON, MASSACHUSETTS

This material is based on work supported by the
Assistant Secretary of Defense for Research and Engineering
under Air Force Contract No. FA8721-05-C-0002 and/or FA8702-15-D-0001.

This report is the result of studies performed at Lincoln Laboratory, a federally funded research and development center operated by Massachusetts Institute of Technology. This material is based on work supported by the Assistant Secretary of Defense for Research and Engineering, ASD(R&E), under Air Force Contract No. FA8721-05-C-0002 and/or FA8702-15-D-0001. Any opinions, findings and conclusions or recommendations expressed in this material are those of the authors and do not necessarily reflect the views of ASD(R&E).

Massachusetts Institute of Technology
Lincoln Laboratory

Undersea Laser Communications Field Test at the Naval Undersea Warfare Center (NUWC)

A.S. Fletcher
H.G. Rao
N.D. Hardy
C.E. DeVoe
I.D. Gaschits
F. Hakimi
S.A. Hamilton
R.D. Kaminsky
M.S. Scheinbart
T.M. Yarnall
Group 67

J.G. Ingwersen
Group 71

Technical Report 1213

30 August 2016

Lexington Massachusetts

This page intentionally left blank.

EXECUTIVE SUMMARY

MIT Lincoln Laboratory conducted a successful field demonstration of narrow-beam laser communications (lasercom) from 28 March–1 April 2016 in the Narragansett Bay, RI, in collaboration with the Naval Undersea Warfare Center (NUWC) Newport. The demonstration achieved real-time communication through turbid harbor waters utilizing a green (515 nm), low-power commercial laser and commercial detectors. Using a single-photon sensitive commercial photomultiplier tube (PMT), we demonstrated communication rates between 0.7 and 8.7 megabits per second (Mbps) with a sensitivity of better than 1.5 detected photons per bit. In the second communication demonstration, we used a wide-bandwidth commercial avalanche photodiode (APD) to achieve 125 Mbps communication rates. In addition to the communication demonstration, high-resolution imaging cameras characterized the laser beam propagation through the harbor waters, providing valuable data to inform lasercom systems design. The field test was a successful proof of concept demonstration and provided key milestones toward a high-performance lasercom terminal suitable for a mobile undersea platform.

In the field demonstration, transmit and receive hardware were placed in watertight containers attached to the ends of an aluminum truss. The truss assembly was lowered into the water and secured against the pilings of a pier in the Stillwater Basin facility of NUWC Newport. The transmitter launched a low-power (0.25 mW), 0.5 cm diameter collimated laser beam into the water. By observing the response of a focal-plane camera in the receive terminal, the transmit beam was manually steered to couple the light into a 2 cm aperture in the receive container. After initial alignment, the beam remained stably pointed from the transmitter to the receiver. The receiver split the light between four sensors: a camera imaging the focal plane, a camera imaging the pupil plane, a PMT detector for high-sensitivity communications, and an APD detector for high-bandwidth communication. The field test provided an important proof of concept for narrow-beam undersea lasercom. Major accomplishments included

- Highly sensitive (power-efficient) communications between 1–8.7 Mbps through 8–12 extinction lengths of harbor water utilizing a single-photon sensitive PMT;
- A real-time PMT transceiver that implemented modulation, demodulation, synchronization, and forward error correction (FEC) encoding and decoding in real-time electronics utilizing a field-programmable gate array (FPGA);
- Robust operation through varying channel conditions, including day, night, and high and low tides;
- APD communication demonstration at 125 Mbps through 5 extinction lengths of harbor water;
- Manual acquisition of a narrow laser beam and stability through natural waters; and
- Channel characterization measurements that support theoretical propagation predictions.

This page intentionally left blank.

ABSTRACT

Narrow-beam laser communication (lasercom) has the potential to maximize both the achievable range and data rate of undersea optical communications. MIT Lincoln Laboratory conducted a field demonstration of narrow-beam undersea lasercom from 28 March–1 April 2016 at the Naval Undersea Warfare Center (NUWC) in Middletown, RI. Transmit and receive hardware were placed in two watertight containers and attached to the ends of an aluminum truss, which was lowered alongside a pier into the Narragansett Bay. A green (515 nm wavelength) collimated laser beam was modulated and steered into a receiver with four sensors: two cameras to provide alignment and beam characterization data and two photodetectors to provide distinct high-speed communications demonstrations. The first demonstration utilized a single-photon sensitive photomultiplier tube (PMT) and achieved data rates up to 8.7 megabits per second (Mbps) over a distance of 7.6 meters, which corresponded to between 8–12 beam extinction lengths. The PMT demonstration included real-time electronics to perform synchronization and forward error correction and achieved a sensitivity of better than 1.5 detected photons per bit. In the second demonstration, a 125 Mbps communications link was demonstrated over 4.8 meters (5 beam extinction lengths) with an APD receiver. Communications and characterization data were collected through a variety of conditions over the five-day field experiment, including day and night, calm and high winds, and flood and ebb tide; robust communication performance was achieved throughout. In the experiment the transmit power, receiver field of view, and link distance were varied. The water transmissivity and volume scattering function were measured throughout the experiment to calibrate the results. The field test data for both communication and beam propagation characterization provide in-water validation of model-generated lasercom performance predictions.

This page intentionally left blank.

ACKNOWLEDGMENTS

The authors would like to thank the Christopher Patty and Richard Kaiser at the Naval Undersea Warfare Center (NUWC) in Middletown, RI, for their essential support in carrying out the field test. Particular thanks also go to the crew that operates the Stillwater Basin facility.

Thanks also go to Joe Scozzafava of MIT Lincoln Laboratory for wise counsel throughout the preparation of the field test.

This page intentionally left blank.

TABLE OF CONTENTS

This page intentionally left blank.

LIST OF ILLUSTRATIONS

LIST OF ILLUSTRATIONS
(Continued)

LIST OF ILLUSTRATIONS
(Continued)

This page intentionally left blank.

LIST OF TABLES

This page intentionally left blank.

1. INTRODUCTION

Undersea optical communication has the potential to revolutionize communication between undersea platforms. Visible light, especially of blue and green wavelengths, propagates through the challenging medium of natural waters with relatively low loss (compared to most electromagnetic frequencies). With terahertz (THz) of bandwidth available, an optical communication system could provide megabit- to gigabit-per-second (Mbps to Gbps) data rates over distances varying from 10s to 100s of meters. These data throughputs are many orders of magnitude greater than alternate undersea wireless options, such as acoustic or very low frequency (VLF). Narrow-beam laser communication (lasercom) is of particular interest as narrow beams enable both the longest distance as well as the highest-bandwidth undersea optical links. MIT Lincoln Laboratory has undertaken a test campaign to explore and develop narrow-beam optical communication for the undersea environment.

The undersea channel suffers attenuation due to absorption and scattering, an exponential process with propagation length with rate parameter c [m^{-1}]. For a narrow field-of-view receiver, the total received energy follows Beer's law as $I(z) = I_0 e^{-c\,z}$, where z is the propagation length and I_0 is the transmitted intensity. The attenuation coefficient is the measure of the water's transmissivity and can also be expressed in terms of the extinction length, $L_{ext} = c^{-1}$ [m], which is the distance at which the light is attenuated by e^{-1}(4.34 dB). For context, a harbor extinction length at green wavelengths is typically between 0.5 and 1 meter; a clear ocean extinction length at blue wavelengths can exceed 20 meters.

Figure 1 compares the range and data rate achieved by a representative selection of published undersea optical communications demonstrations [1–7]. The range is normalized by the number of extinction lengths of water, thus providing a relevant comparison of highly attenuating harbor demonstrations with demonstrations in the relatively low attenuation of clear ocean water. The in-water demonstrations typically utilized a wide transmit beam from a light-emitting diode while the high-data-rate laboratory demonstrations used a collimated laser beam. While a wide transmit beam simplifies signal acquisition and tracking, it limits both the achievable range and data rate. The red dashed curve in Figure 1 represents the predicted achievable performance for a small narrow-beam lasercom terminal; 100+ Mbps class links are possible at more than 20 extinction lengths.

From 28 March–1 April 2016, MIT Lincoln Laboratory conducted an in situ field experiment and demonstration of narrow-beam undersea laser communication (lasercom). The experiment was conducted in the Narragansett Bay, Rhode Island at the Naval Undersea Warfare Center (NUWC) Newport. This technical report presents a description of the experiment and a summary of the collected results.

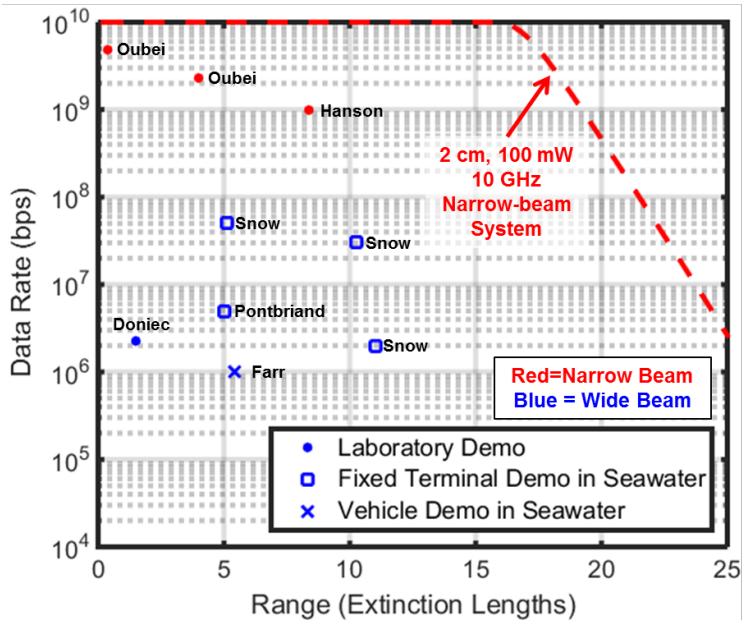

Figure 1. Selection of published undersea optical communications demonstrations.

The field experiment had two principal objectives. The first objective was to conduct a real-time demonstration of narrow-beam lasercom through natural waters. As part of the objective, the demonstration would produce a transceiver design as a building block for a prototype lasercom terminal. The second objective was to characterize the propagation of a narrow-beam laser through harbor water and measure the communication impact of transmitter and receiver design elements. In-water characterization data is vital to guide lasercom terminal design.

The field experiment achieved both objectives. As will be detailed in this report, real-time communications were achieved between 0.7 Mbps and 8.7 Mbps over a distance of 7.8 meters with single-photon sensitivity. The demonstrated distance corresponds to 8–12 extinction lengths due to the high attenuation of harbor water. A real-time demonstration of 125 Mbps with a wide bandwidth photodetector was achieved over a distance of 4.8 meters (5 extinction lengths). Additionally, laser propagation measurements were carried out with high-resolution imaging of both the focal plane and receive aperture plane.

The technical report is organized as follows. Section 2 describes the hardware and infrastructure of the field test. Section 3 describes the specific experiments carried out and the corresponding conditions. Section 4 describes the data results and provides summary data analysis.

2. FIELD TEST HARDWARE AND INFRASTRUCTURE

This section describes the systems utilized in the field test, including the relevant performance specifications. We begin with a system overview and the infrastructure supporting it. We follow with details of the optical, electrooptical, and electronic components of the field test. We conclude the section describing the equipment for measuring the water transmissivity and scattering characteristics.

2.1 SYSTEM OVERVIEW

The field test concept is simple: an optical transmitter and optical receiver were rigidly mounted to a structure and placed in the water to demonstrate optical communication and characterize beam transmission. The block diagram for the optical transmitter is shown in Figure 2. Transmitter block diagram.. The principal components were a fiber-coupled green laser, a variable optical attenuator, and optics to launch and steer a collimated beam.

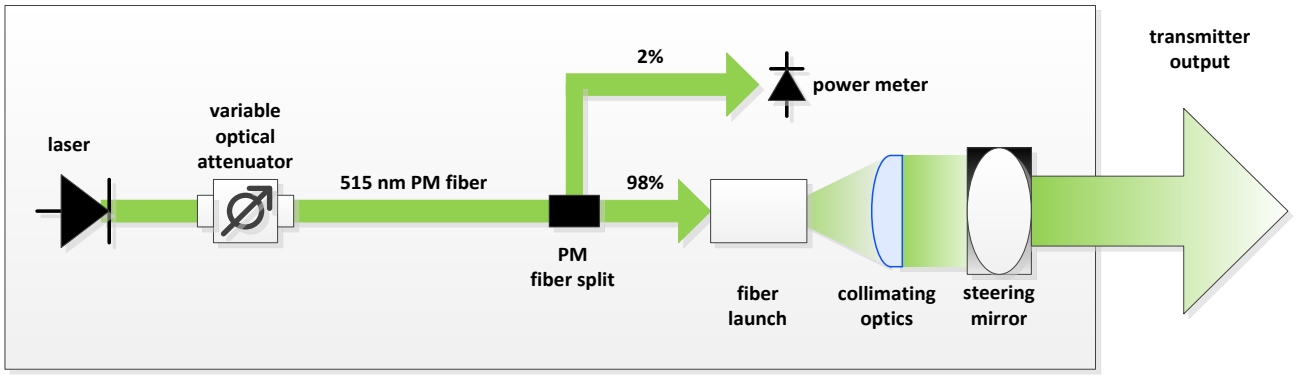

Figure 2. Transmitter block diagram.

The receiver block diagram is given in Figure 3. Receiver block diagram.. The light was collected in an aperture and split between four sensors. Two sensors were cameras, one imaging the focal plane and the other the pupil (or aperture) plane of the receiver. These sensors were used to characterize the beam propagation, including providing the signals needed to align the transmitted beam to the receive sensors. There were also two photodetectors – a photomultiplier tube (PMT) sensitive to single photons and an APD with a wide-bandwidth response – used in the communications demonstration. Both detectors and the pupil-plane camera were behind a mechanical iris that controlled the sensors' field of view.

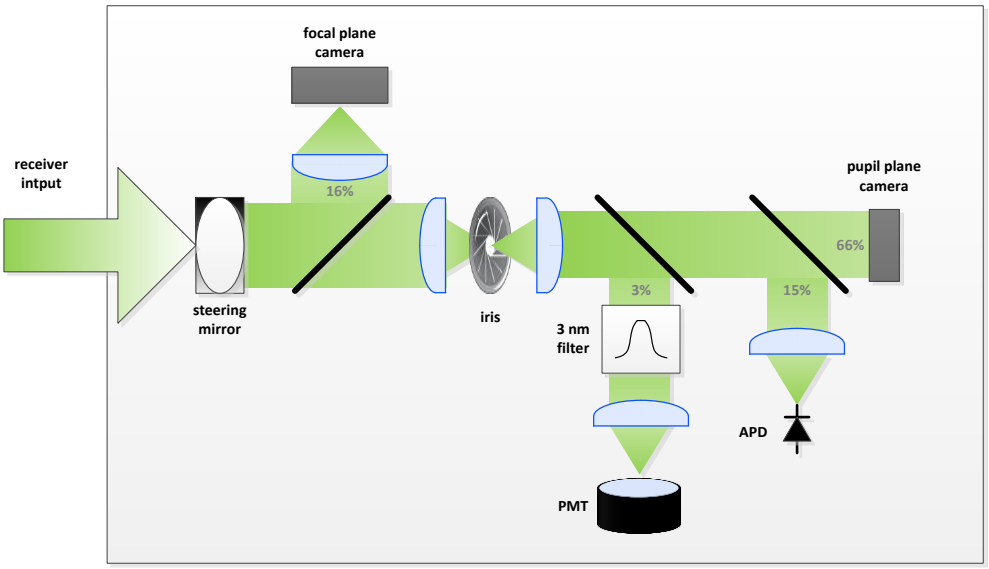

Figure 3. Receiver block diagram.

Transmit and receive hardware were housed in watertight containers fixed to opposite ends of an aluminum truss. The truss assembly was lowered into the water alongside the pier and held in place against the pilings. (See Figure 5 and Figure 5 for an illustration and photograph of the truss assembly.) Both the transmit and receive containers were connected to a control center on the pier with power cables and optical fibers.

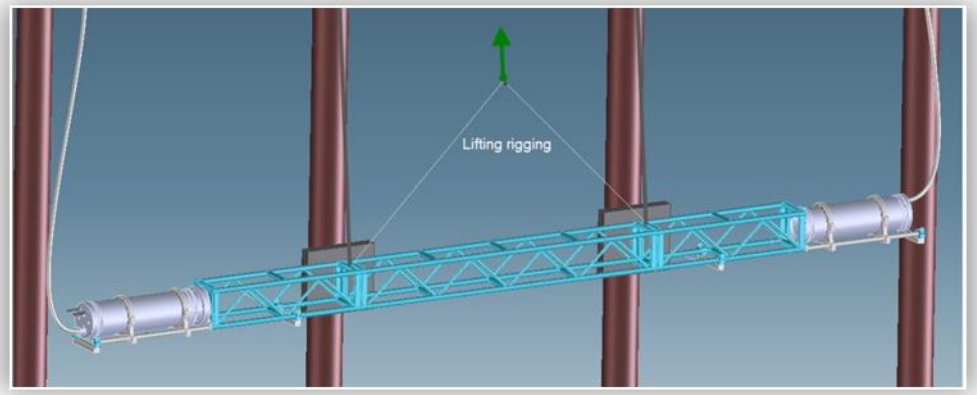

Figure 4. CAD drawing of truss assembly alongside pier pilings.

A small trailer on the pier (seen in the background of Figure 5) housed the control center for the field experiment. The control center included computers to remotely command and monitor the experimental subsystems. Additionally, some transmit and receive hardware (such as a laser and variable optical attenuator) remained on shore and were connected to the submerged hardware via optical fiber. The details of the subsystems will be described in the following sections.

Figure 5. Truss assembly being removed from the water of Narragansett Bay, RI, on 31 March 2016.

2.2 OPTICS DETAILS

2.2.1 Transmitter Optical Chain

The onshore components of the optical system consisted of the transmit laser and a variable optical attenuator (VOA). The onshore components were connected to the transmit container's optical assembly via a 30 m Nufern PM-S405-XP+ fiber. Inside the transmit container, the optics consisted of a polarization-maintaining fiber power tap connected to a Thorlabs power meter, a collimating lens, and a 1″ piezo steering mirror. During system assembly, the continuous wave (CW) power at the fiber input to the VOA was measured to be 17.8 mW (12.5 dBm). The loss going through the VOA, the optical fiber, collimating optics, and transmit window contributed a loss of ~15 dB, reducing the power measured in air to 0.59 mW (–2.3 dBm). When modulated, the measured power was reduced to 0.27 mW (–5.7 dBm). The beam exiting the transmit fiber was collimated with a 23 mm focal length lens, yielding a mode field diameter of 5.5 mm.

2.2.2 Receiver Optical Chain

The receiver chain consisted of a steering mirror, three polarization-sensitive beamsplitters that directed the received beam to the four different sensors, a field-restricting iris, focusing lenses, and a bandpass filter. The optics used had diameter of 2.54 cm (1″). The receiver block diagram is shown in Figure 3; a photograph of the assembled receiver optical chain is given in Figure 6.

The split ratios for the three beamsplitters, assuming a polarized beam, were chosen to allow each sensor to operate comfortably within its dynamic range. The nominal split ratios are given in Figure 3. The throughput of the receiver optics as measured for the expected polarization state (parallel to the optical bench, p-polarized) is listed in Table 1.

TABLE 1

Receiver Beamsplit Measurements

	Throughput (dB)			
	Focal Plane Camera	PMT	APD	Pupil-Plane Camera
P-Polarized (nominal)	–8.8	–17.3	–9.8	–2.9

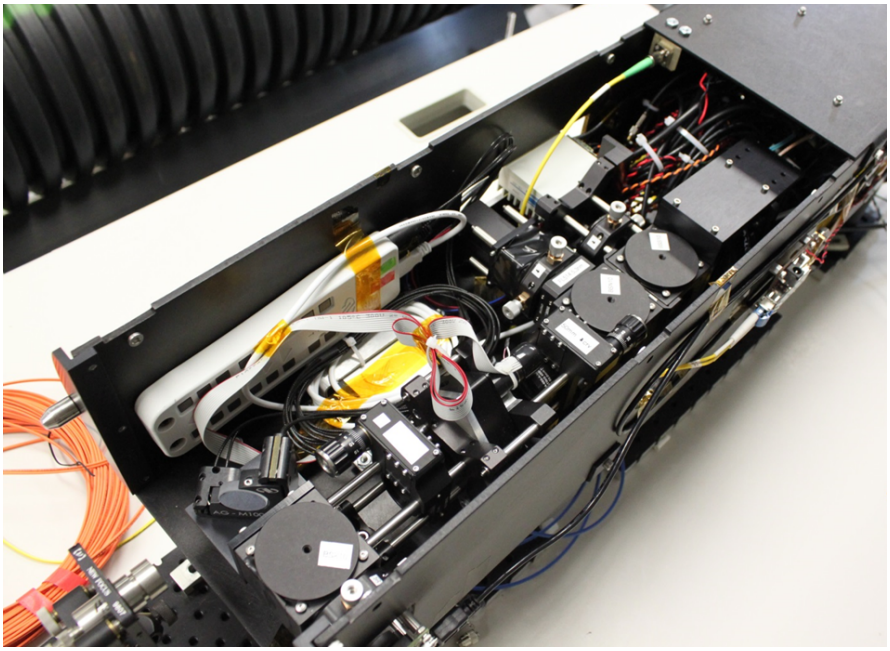

Figure 6. Optical and electrooptical components as integrated onto the receive chassis.

Each sensor had a nominal field of view set by the sensor size and the focal length (if applicable) of the lens used to concentrate the received beam. Table 2 lists the sensors' fields of view with the iris fully open. The characterization camera is nominally located at the pupil plane, and thus its field of view is only limited by the geometry of the system (vignetting) and the iris opening.

TABLE 2

Sensor Field of View

Sensor	Active Area (mm)	Lens Focal Length (mm)	Full Field of View (mradians)
Alignment Camera	5.3 × 6.6	30	177
APD	0.5	40	12.5
PMT	8	50	160
Characterization Camera	25.7 × 27.25	NA	Limited only by iris and vignetting

Located after the alignment beam splitter, between two lenses, the iris was used to limit the field of view of the two detectors and the characterization camera. The IMS-25A Pacific Laser Equipment motorized iris utilized a stepper motor to open the iris from fully closed (no light passes) to a maximum diameter of 25 mm. The smallest useable size was approximately 50 µm (1 mrad FOV). At the small iris settings, the opening had an asymmetric appearance due to the leaf design of the iris. Figure 7 shows pictures of the iris set at openings of roughly 0.1 mm and 1 mm (~2 mrad and ~20 mrad). As the iris opens up, the opening becomes significantly more symmetric.

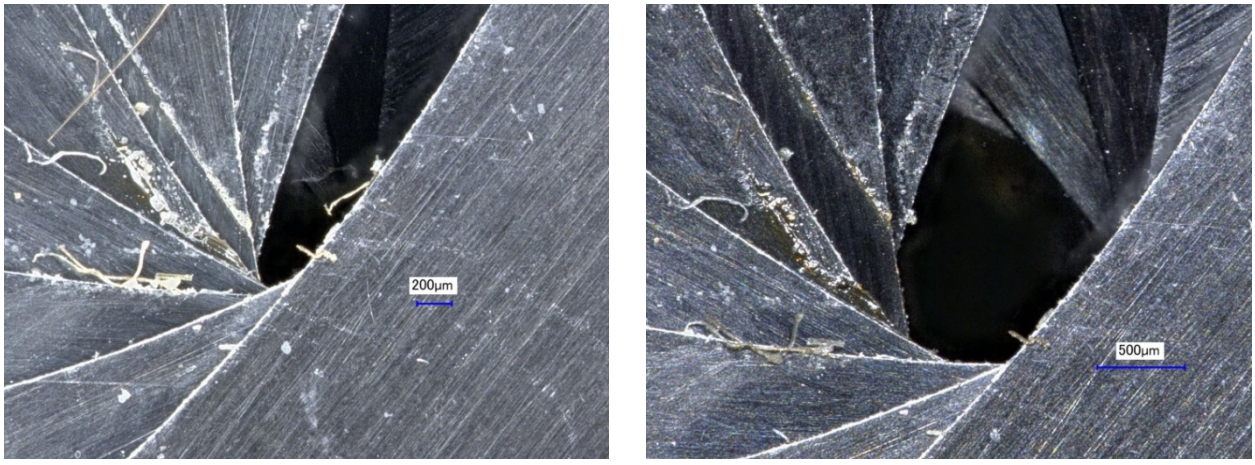

(a) (b)

Figure 7. Microscope image of the iris opening at settings of (a) 0.1 mm and (b) 1 mm, corresponding to approximately 2 mrad and 20 mrad fields of view.

2.3 ELECTROOPTICS COMPONENTS

2.3.1 Transmit Laser

Figure 8. Toptica "iBeam smart – Compact Diode Laser."

The transmit laser was Toptica "iBeam smart – Compact Diode Laser" operating at 515 nm. A Toptica fiber coupler ("SmartDock") was added for high-efficiency coupling of the laser free-space beam into fiber cables. The fiber cable was polarization maintaining (PM) with operating range of 460–700 nm with mode field diameter 2.4 μm @488 nm, NA = 0.12. The laser linewidth was 1 nm. The laser could be modulated up to 250 MHz. A list of laser specifications is given in Table 3; these are nominal values from the manufacturer.

TABLE 3

Toptica Laser Characteristics (from Manufacturer Data Sheet)

Center wavelength	515 nm
Optical linewidth	1 nm
Spatial mode	$M^2 < 1.2$
Beam divergence	<1 mrad
Beam diameter	1 mm
Free-space optical output power (*maximum*)	100 mW
PM fiber-coupled optical power (*maximum*)	50 mW
Digital modulation bandwidth	250 MHz
Optical pulses rise and fall time	<1.5 ns
Laser head dimensions (H × W × D)	40 × 40 × 100 mm
with SmartDock	40 × 40 × 151.5 mm

2.3.2 Communication Photodetectors

The two photodetectors used in the communication demonstration are pictured in Figure 9. An APD silicon high-speed photodetector, specifically the Hamamatsu C5658 APD, was used for 125 Mbps data transmission. The detector high-band cutoff frequency is 1000 MHz and low-band cutoff frequency is 50 kHz. The effective active area diameter is 500 μm. The APD internally multiplies the photocurrent with a gain of ~100 followed by a low-noise amplifier. Typical photoelectric sensitivity of the detector is 2.5×10^5 V/W; the detection limit of the unit is –48 dBm. The APD detector was followed up by a 95 MHz Chebyshev filter. Figure 10(a) shows the APD's output at 250 Mbaud. (The rate was limited by the laser.) The APD yields open eyes, which can be easily corrected by FEC.

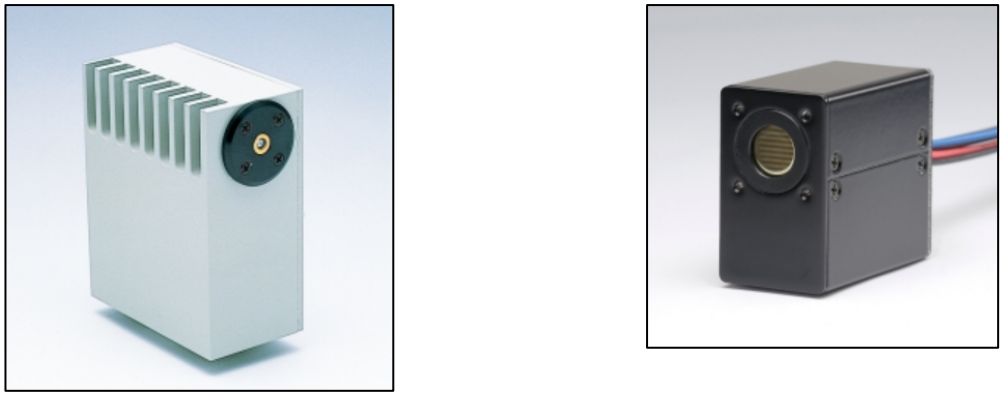

(a) **(b)**

Figure 9. Communications photodetectors: (a) Hamamatsu C5658 APD and (b) Hamamatsu H10682-210.

The photon counting detector used was a Hamamatsu H10682-210, pictured in Figure 9(b). The unit consists of metal package photomultiplier tube, high-speed photon counting circuit, and a high-voltage power supply. The high-voltage supply for the PMT and the discrimination level are preset to optimum values, allowing photon counting measurement by connecting a +5 V supply. The photocathode material is ultra bialkali (UBA) for higher sensitivity than conventional photon counting heads. The photocathode area is round with an 8 mm diameter. The unit also has an over-light detection function to output a signal indicating count reductions due to excessive incident light. The typical count sensitivity around a wavelength of 500 nm is 4.6×10^5 $s^{-1}pW^{-1}$. The PMT had a measured dark count rate of 20 Hz, a rise time of 1.5 ns, a pulse pair resolution (i.e., dead time) of 20 ns, and a quantum efficiency of approximately 10% at the signal wavelength. Figure 10(b) shows the PMT's linearity vs. input power and the output signal for high input power. At saturation, the PMT count rate is approximately 18.3×10^6 Hz.

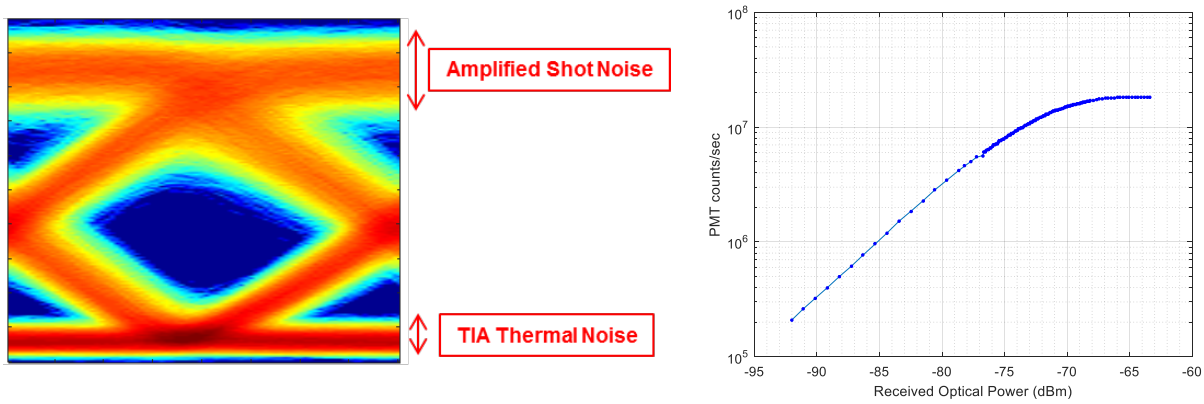

(a) (b)

Figure 10. (a) 250 Mbaud eye diagram from APD output. (b) Measured PMT count linearity vs. input power.

2.3.3 Cameras

Two cameras were used for system alignment and beam characterization (both are shown in Figure 11). The Edmund Optics EO-1312M 1/1.8″, CMOS Monochrome camera imaged the focal plane and was used especially for system alignment. It is a progressive scan complementary metal–oxide–semiconductor (CMOS) with a sensing area of 6.79(H) × 5.43(V) mm, and 1280(H) × 1024(V) pixels with size 5.3×5.3 µm and pixel depth of 8 bits. The maximum frame rate is 25 fps.

The pupil-plane characterization camera, a XIMEA MH110MC-KK-FA, is an 11 megapixel (4008 × 2672 pixels) low-noise, charge-coupled camera. It is monochrome with a sensor area of 25.7 × 37.25 mm and 9 µm pixel size. Read-out options are 8, 10, 12, or 14 bits per pixel, with a dynamic range of 70 dB and a frame rate of 2 fps (at maximum resolution).

(a) (b)

Figure 11. Characterization cameras: (a) Edmund Optics EO-1312M and (b) XIMEA MH110MC-KK-FA.

2.4 ELECTRONICS

This section describes the electronics for the communication transceiver. As the transceiver is a pathfinder for a future lasercom prototype terminal, we start by listing the system requirements and the corresponding design goals for the communications demonstration.

2.4.1 Communication Demonstration Goals and System Considerations

Wide Dynamic Range Transceiver An undersea terminal is expected to operate over an extensive range – potentially 90 dB – of receiver signal levels. For this reason, the communications demonstration has two operating modes: a high data throughput case (125 Mbps) with high signal levels, and a lower data rate (1–10 Mbps) with lower signal levels.

Operation through Natural Waters An undersea terminal must robustly function in natural conditions, including background light and signal blockages. For this reason, the real-time transceiver for the PMT link pursued synchronization and link establishment that was robust to link outages. Additionally, the transceiver adapted performance to the background light observed during operation.

Low Size, Weight, and Power (SWaP) Undersea terminals, especially for unmanned underwater vehicles, are likely to be both size and power constrained. While the demonstration itself was not constrained to low SWaP, the transceiver design pursued highly efficient solutions to minimize the required transmit power and terminal size. Specifically, this drove the utilization of advanced FEC codes.

The system requirements for the transceiver electronics may be summarized as:

- Real-time data generation and reception at multiple channel rates (approximately 1–125 Mbaud)
- Photon-counting and linear optical detectors
- Burst-mode synchronization
- Automatic channel rate estimation
- Automatic channel estimation (background and signal light levels)
- Soft-decision FEC with run-time control of code rate
- Compatibility with future requirements for interleaving and retransmission.

2.4.2 Overview of Communication Links

The transmit laser was on-off key (OOK) modulated with the source data. Separate waveforms and modulation electronics were used at the transmitter and receiver depending on whether the experiment received the signal with the PMT or the APD. Figure 12 shows a simplified description of the transmitter and receiver signal chains for (a) the PMT and (b) the APD. In both cases, the links ran continuously in real time. A variable attenuator was used to control the amount of power delivered to each receiver. The PMT link utilized FPGA boards for the transmit and receive electronics, representing a mature development of real-time modem functionality. The real-time APD link utilized laboratory-grade equipment, namely a bit error rate tester (BERT) to generate the data and perform real-time demodulation and an oscilloscope to capture the signal detector output for post-processing (when applicable).

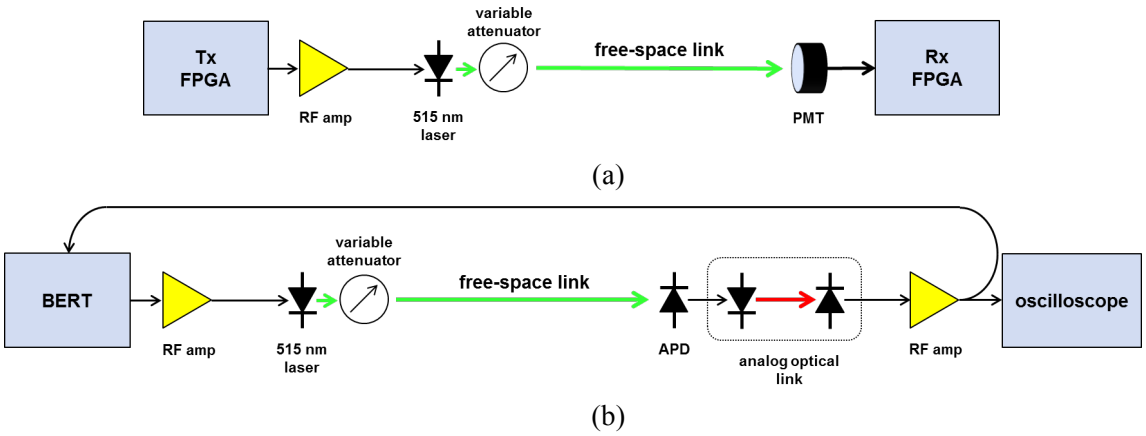

Figure 12. Simplified overview of (a) the PMT transmitter and receiver signal chain and (b) the APD transmitter and receiver signal chain.

2.4.3 PMT Link Details

For the PMT receiver, all functions (synchronization, rate estimation, channel estimation, and soft-decision decoding) were implemented in the receiver FPGA. The overall hardware footprint is therefore small due to the mature transceiver design. The FPGA code was written in the industry-standard languages Verilog and VHDL, which allows it to be ported to other platforms. For the PMT communication waveform, we utilized a high duty-cycle return-to-zero (RZ) format, which has a clock frequency component. The signaling occurred at one of three data rates: 10.4, 5.2, or 1.3 Mbaud.

Figure 13 shows the structure for a single frame. The header bits are used for alignment and other management functions. During the field test, only the frame alignment sequence (FAS) and frame sequence number (FSN) fields were utilized. The FAS is a fixed 96-bit pattern that is used to indicate the start of each frame. The FSN contains a 22-bit message protected by forward error correction. The payload's code rate is transmitted within the frame so that the code rate can be changed on a frame-by-frame basis. Along with automatic channel rate detection, this allows the communication link to adapt without requiring a side channel. The FEC protection allows robust reception with a channel bit error rate (BER) as high as 27%.

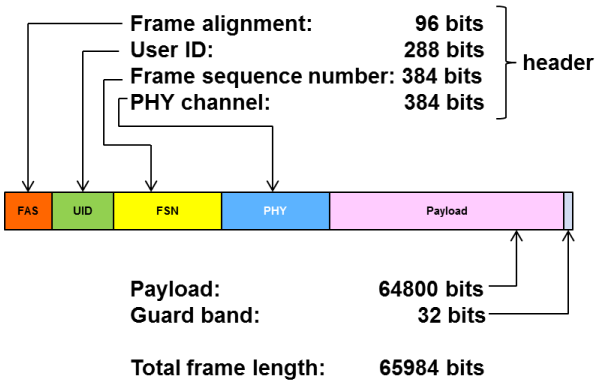

Figure 13. Frame structure for PMT link.

2.4.4 APD Link Details

The electrooptic and electronic receive chain for the 125 Mb/s OOK undersea link begins with a linear-mode avalanche photodiode. The APD converts the optical signal to an electrical signal by producing an electrical current in response to incident light via an avalanching process in a strongly reverse-biased active region of silicon. The electrical current then continues to a transimpedance amplifier (TIA), a device that transforms current signals into more manageable voltage signals. The noise of the avalanche process and the thermal noise at the input of the TIA set the noise floor of the system. The Hamamatsu C5658 comprises these three functional blocks – the silicon detector, the high-voltage bias,

bias, and the TIA – in a small form-factor package. Following the output of the TIA is an RF amplifier that serves to boost the voltage signal before filtering and measurement.

The modulation format chosen for the APD link was non-return-to-zero on-off keying (NRZ-OOK). The BERT generated a 2^7–1 pseudo-random bit stream at 125 Mbaud. At the time of the field demonstration, the APD receiver was not developed to the same maturity level as the PMT receiver. For this reason, the raw output of the APD was transmitted back above the water for processing. A linear optical link operating at 1.5 μm over single-mode fiber was used for this purpose. Once received above water, the RF output of the APD was filtered using a second-order Bessel–Chebyshev low-pass filter with a 3 dB cutoff of 78 MHz. The BERT's input acted as a 1-bit comparator on the amplified APD output. The amplified APD output was also monitored by an oscilloscope to obtain noise statistics.

2.4.5 Field Test Implementation

The BERT, transmit FPGA, transmitter amplifiers, 515 nm laser, and variable attenuator were located above the water. Figure 14 shows a block diagram of the submerged transmitter enclosure.

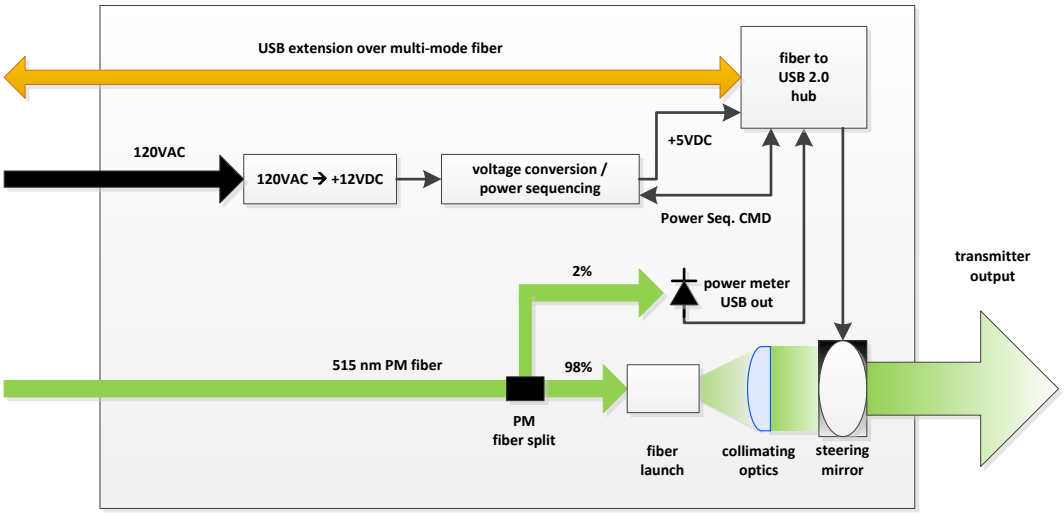

Figure 14. Block diagram of submerged transmitter enclosure.

The 515 nm modulated signal was sent down to the transmitter enclosure via a polarization-maintaining (PM) fiber. The launch power was monitored using a USB-connectorized power meter, and the output signal was steered via a mirror with a USB interface. A USB fiber extender was placed inside the enclosure. This extender acted as a USB extension cable, transporting USB commands to the mirror and power meter over multi-mode fiber. The extender also acted as a USB hub. The enclosure was powered by 120VAC sent down from above the water. With this approach, the number of external

connections to the enclosure could be minimized to two fibers and a power cable. Furthermore, the USB fiber extender allowed a desktop computer to control the USB devices inside the enclosure as if they were above the water.

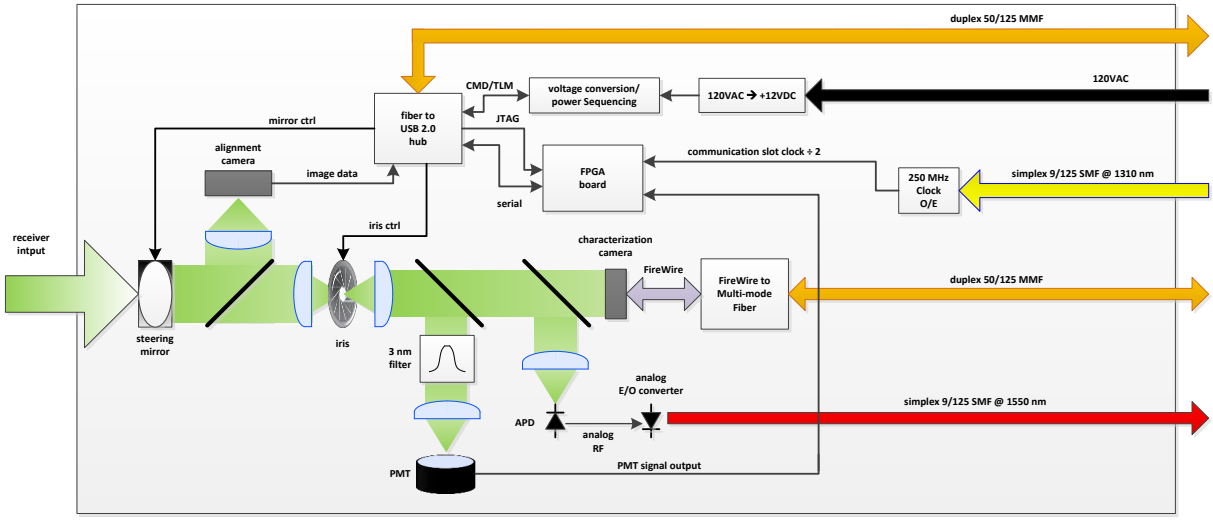

Figure 15. Block diagram of submerged receiver enclosure. MMF = multimode fiber; SMF = single-mode fiber.

The receiver enclosure hardware is shown in Figure 15. The PMT signal was handled by a Xilinx VC707 Virtex 7-based FPGA board inside the enclosure. A USB fiber extender/hub was used to transport USB control from the desktop control computer above the water to USB elements within the enclosure. Additionally, a FireWire extender was incorporated to transport the output of the beam characterization camera to the desktop computer. The receive end of the analog optical link, the associated RF post-amplifier, and oscilloscope were located above the water.

2.5 WATER TRANSMISSIVITY MEASUREMENTS

Water transmissivity was measured in three ways during the field test: an aquarium measurement, a measurement with a commercial sensor, and analysis of the count rates on the PMT detector. These three methods will be described below.

2.5.1 Aquarium Transmissometer

Water was removed from the harbor and placed in a glass aquarium. A green laser was shined through the aquarium and the resulting power level was measured. This power level was compared to attenuation through air, giving a measure of the attenuation due to the water. The laser was at the same wavelength as communication laser, but the water was taken from the top layer, while the communication

system was submerged several feet. Additionally, the sensor collected a significant portion of the forward-scattered light, implying that it would underestimate the scattering coefficient.

2.5.2 LISST-100X

Our second measurement apparatus was a Sequoia Scientific LISST-100X sensor, a submersible multiparameter system that operates at 670 nm. The LISST-100X was attached directly to the truss (Figure 16) and the volume scattering function, attenuation coefficient, temperature, and depth were recorded throughout operations. This sensor provided measurements of c at the same depth as the submerged hardware, though on a different wavelength from the communication laser. While the total amount of scattering is expected to be similar, the absorption is typically higher for the longer wavelength.

Figure 16. LISST-100X mounted to the truss assembly.

2.5.3 PMT-Derived Transmissivity Measurement

The third transmissivity measurement uses the output of the PMT – the photon-counting communication detector – to determine the attenuation coefficient. By characterizing the transmitter and receiver response (optical splitting ratio in the receiver container, total transmitted power, detector response, etc.), this can then give an accurate estimate of c.

3. FIELD TEST TIMELINE

This section describes the field test experiments conducted each day.

TABLE 4

Timeline of Field Test

Date	Task
28 March 2016	Equipment was shipped and assembled at NUWC.
	An initial measurement of water clarity was made with the aquarium transmissometer. The observation led to a truss assembly length of 25 feet, placing the transmit and receive windows at a distance of 25.7 feet (7.83 m). This was estimated at 9.2 extinction lengths.
29 March 2016	The truss assembly was completed and wrapped with black nylon netting to prevent large detritus or fish from entering the beam.
	The truss assembly was lowered into the water around 3:30 PM. It was positioned against the dock pilings and suspended 1–2 feet from the sea floor.
	Using the focal plane imager, the transmit mirror was manually adjusted to steer the beam into the receive optics. The pupil-plane imager and the mechanical iris were then used to fine tune the alignment.
	The first communication tests were performed utilizing the PMT receiver. Error-free communication was achieved at 10.7 Mbaud signaling with a ½-rate FEC, achieving 5.35 Mbps communication. The communication performance was characterized by sweeping the VOA settings from high attenuation through to nearly zero attenuation.
	Additional PMT communications experiments were conducted after sundown on 29 March. During the evening tests, the floodlights on the dock were turned off, minimizing background light to the communication link.
30 March 2016	Characterization results were recorded with the pupil-plane imager at various iris settings. Additionally, a series of focal plane images was taken over a variety of exposure times to quantify the light that was arriving off-axis.
	PMT communications measurements were recorded at several iris settings and data rates.
31 March 2016	Between 9 AM and 10 AM, the truss was removed from the water. It was reassembled with 15 feet of length (15.75 feet, or 4.8 m, from window to window) and returned to the water. Additionally, the black fabric was removed from the truss.
	The APD communication mode was demonstrated in real time with the BERT. The link ran at a 125 MHz modulation rate and there were two observed errors in 1 minute (7.4e9 bits) for a BER of 2.7e-10.
1 April 2016	The truss was removed from the water.

3.1 WEATHER CONDITIONS

Weather data for the duration of the field test was compiled from the public record of the National Weather Service (hosted by MesoWest at the University of Utah). The weather station is located at the KUUU Rhode Island state airport facility located 1.5 miles east of the Stillwater Basin test site. The weather conditions are presented in Figure 17.

During the first day of testing, 29 March 2016, mostly clear weather was observed with occasional clouds moving in and out. The minimum and maximum air temperature was between 38°F and 52°F with relative humidity varying between 37% and 60%. Moderate to strong winds were recorded in the range of 12 mph and 21 mph with wind gusts between 26 mph and 24 mph. The wind direction was steady between WNW (290 degrees) and NNW (340 degrees).

During the second day of testing, 30 March 2016, clear weather was observed throughout the day. The minimum and maximum air temperature was between 34°F and 47°F with relative humidity varying between 28% and 56%. The wind speed was between 5 mph and 16 mph with wind gusts between 20 mph and 26 mph. The wind direction was NW (300 degrees) in the morning, changing to SSW (200 degrees) later in the day.

During the third day of testing, 31 March 2016, the weather changed from clear in the morning and during the day to mostly cloudy, overcast, and finally fog in the late evening. The minimum and maximum air temperature was between 47°F and 57°F with relative humidity starting at 83% in the morning, dropping to 64% at noon, and then gradually rising to 93% in the late evening. The wind speed was between 5 mph and 16 mph with wind gusts between 20 mph and 26 mph. The wind speed was between 7 mph and 17 mph with wind gusts between 20 mph and 34 mph from morning to noon, calming down toward the evening. The wind direction was steady SSW (210–190 degrees).

(a)

(b)

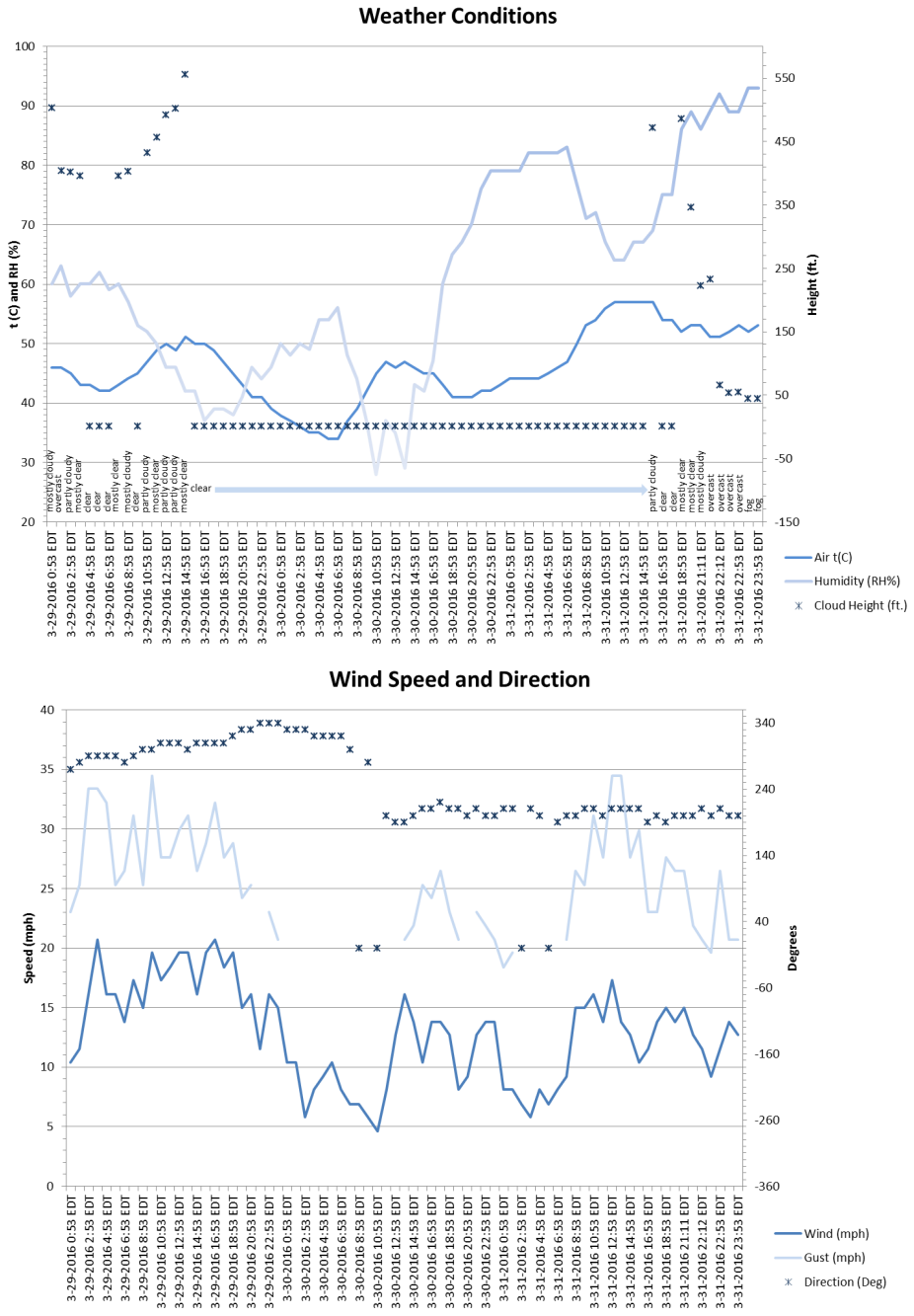

Figure 17. Weather data for 29–31 March 2016. (a) Cloud height, air temperature, and relative humidity. (b) Wind speed and direction.

Table 5 presents the tide data during the field test for the days when in-water data was collected.

TABLE 5

Tide Information during the Data Collection

Date	High Tide		Low Tide	
	AM	PM	AM	PM
29 March 2016	12:01	12:28	5:36	5:37
30 March 2016	12:47	1:19	6:22	6:25
31 March 2016	1:38	2:10	7:22	7:29

4. DATA ANALYSIS

This section presents a summary of the data collected during the field test and an initial analysis.

4.1 TRANSMISSIVITY MEASUREMENTS

4.1.1 Aquarium Transmissometer Data

The aquarium transmissometer was 1.22 m in length, and was filled with two five-gallon buckets that were raised out of the harbor. A laser pointer was first shown onto a Thorlabs LP520-SF15 power meter through air, and then through the aquarium. The relative amount of loss was recorded. Additionally, the aquarium was characterized using pure water to determine how much of the loss was due to reflection from the glass walls. The adjusted attenuation, and the subsequent calculation of c and L_{ext} are shown in Table 6.

TABLE 6

Aquarium Transmissometer Measurements

Day	Time	Loss (dB)	c (m^{-1})
Monday	12:45 pm	–6.26	1.18
Tuesday	8:00 am	–6.36	1.20
	4:00 pm	–8.16	1.54
Wednesday	9:30 am	–7.76	1.47
	10:49 am	–9.76	1.84
	1:40 pm	–8.36	1.58
	3:28 pm	–7.56	1.43
	6:00 pm	–12.66	2.39
Thursday	7:43 am	–7.16	1.35
	11:35 am	–10.96	2.07
	3:15 pm	–11.56	2.18

4.1.2 LISST-100X Transmissometer Data

In Figure 18, we plot the measured value of c from the LISST-100X along with the sensor's depth. We see similar values as were measured in the aquarium, with c ranging from 1 to 2 m^{-1}. We also see an interesting trend, where the amount of attenuation moves linearly with the truss depth. This change in depth is a reflection of the changing tide; it is therefore possible that the attenuation is both a function of the tide and depth.

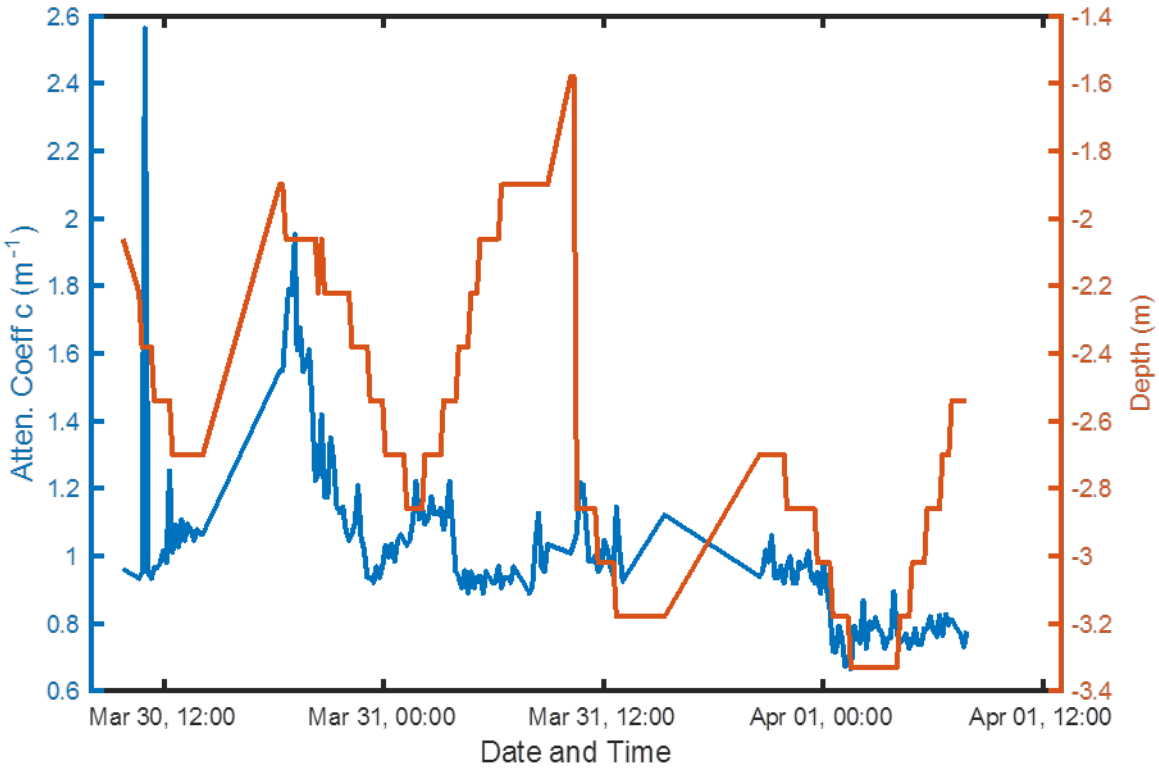

Figure 18. LISST attenuation coefficient and depth measurements.

4.1.3 PMT Transmissometer Data

In Figure 19, we co-plot the PMT-derived attenuation coefficient estimates with those from the other two methods. We see good agreement between the LISST and PMT transmissometer measurements. The aquarium measurement seems to overestimate the attenuation of the water; this is possibly because the water was taken from the harbor surface which contains more biologic scatterers and absorbers.

The PMT communication trial with the maximum attenuation occurred at 6:14 PM on Wednesday, 30 March, which was during low tide. The PMT and LISST both measured an attenuation coefficient of

$c = 1.52$ m^{-1}, yielding an extinction length of $L_{ext} = 0.645$ m. This implies that the link was closed over 11.9 extinction lengths, plus the additional attenuation from energy splitting in the receiver. The attenuation coefficient of 1.43 m^{-1} observed at 5:25 PM on 29 March also occurred at low tide.

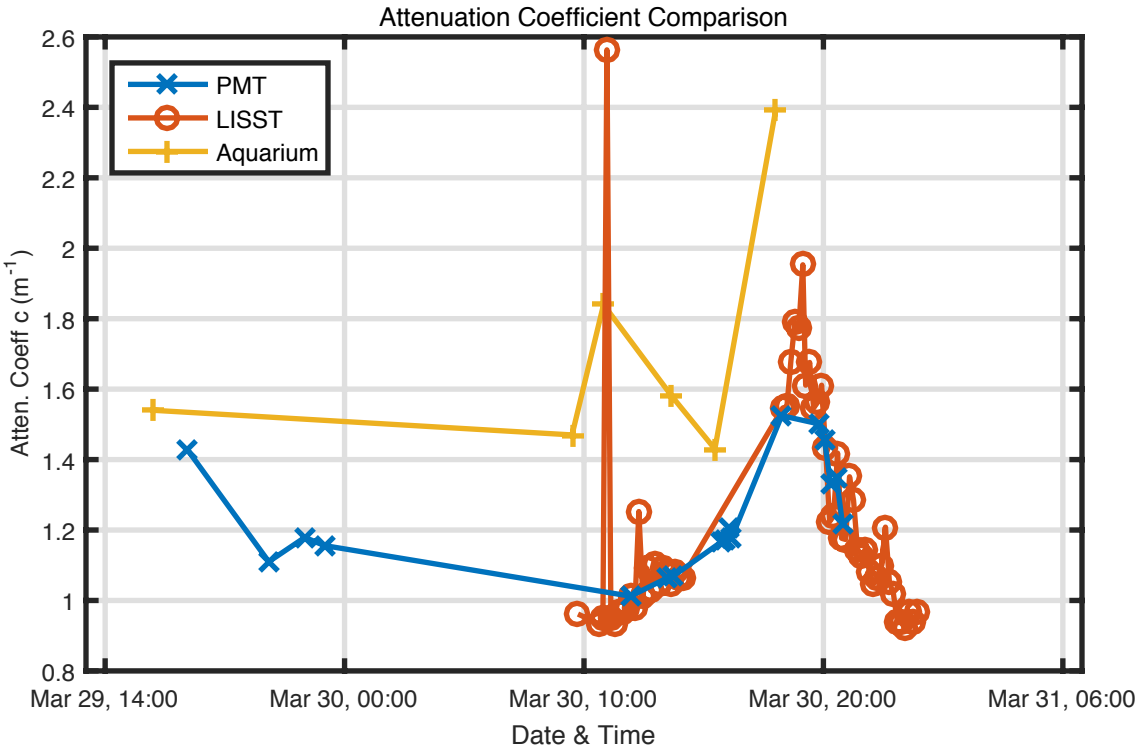

Figure 19. Attenuation coefficient comparison.

4.2 CHARACTERIZATION RESULTS

4.2.1 Comparison to Simulation

In this section, we compare the images taken by the pupil-plane and focal-plane imagers to simulations of equivalent pupil- and focal-plane images predicted by undersea optical propagation models. Several of our experiment design choices – the size of beam, field-of-view filtering, and length of the truss, to name a few – were informed by simulation results. The simulations were for generic "turbid harbor" water with absorption and scattering coefficients $a = 0.366$ m^{-1}, $b = 1.824$ m^{-1}, and thus an attenuation coefficient of $c = 2.19$ m^{-1}, and a single-scattering albedo of $b/c = 0.833$. After the field test, we reran the simulator with the measured c values, but maintaining the same scattering albedo.

The agreement in c values from the LISST and the PMT at different wavelengths suggest that there was a high scattering albedo, similar to the 0.833 used in the simulation.

The angular resolution for the focal-plane imager was chosen to provide a wide field of view so that the beam could be found and aligned once the truss was lowered into the water. A comparison of the simulated and measured focal plane images can be seen in Figure 20 below. This image was taken from the 30 March evening experiments.

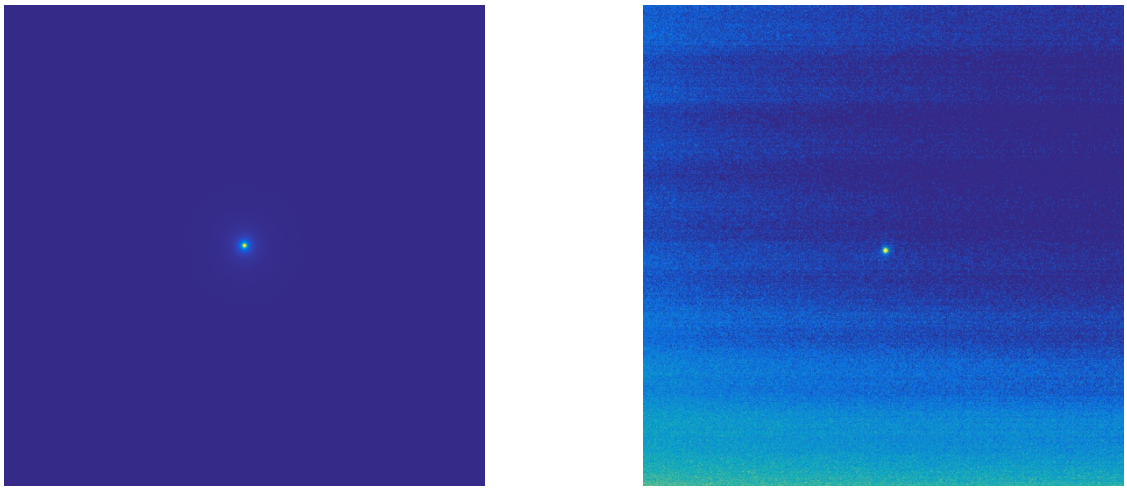

(a) **(b)**

Figure 20. Comparison of focal plane images: (a) image from simulation using the measured field test conditions and (b) image from Edmund Optics camera during the NUWC field test. The NUWC trials saw a uniform background, but the main spot from the transmitted beam matched the simulation.

The pupil-plane imager directly imaged the beam without magnification. However, the received light was first spatially filtered (by the window cover), and then angularly filtered (by the FOV-limiting iris). The windowing appears in the images as a ring around the beam, while the filtering removes most of the scattered and background light. A typical image, also taken Wednesday evening, and its equivalent simulation (with the saturation) are shown in Figure 21.

During the trials, we also saw the beam deviate from the centered, Gaussian shape predicted by simulation. Some of this was beam wander, likely due to motion of the truss. It was generally stronger during low tides, when the truss was closer to the surface and more subject to motion from waves. Additionally, there were several obstructions that moved in and out of the beam. These were most likely jellyfish, which we saw in abundance when raising water out of the harbor to make aquarium transmissometer measurements. Example images of both of these beam deformities are shown in Figure 22.

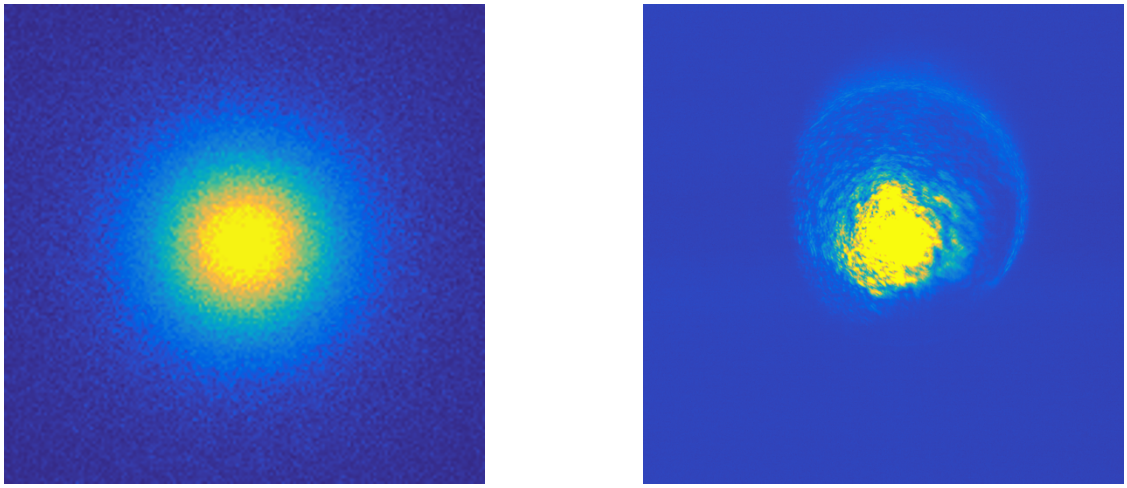

(a) **(b)**

Figure 21. Comparison of filtered pupil-plane images: (a) image from simulation using the measured field test conditions and (b) image from XIMEA camera during the NUWC field test. The NUWC field tests had an aperture that is visible as a faint ring around the main beam, while the simulation had no spatial constraint, and thus let in more scattered light.

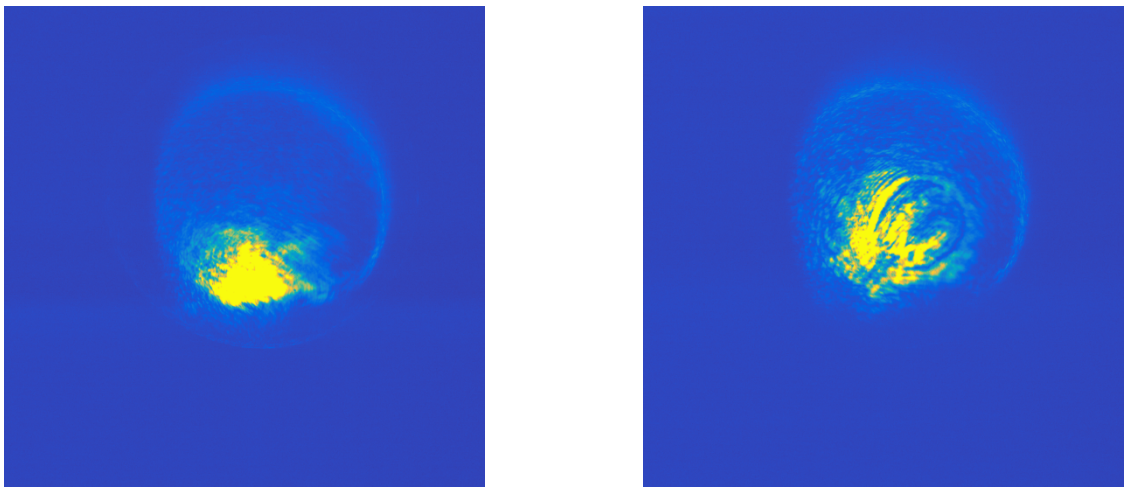

(a) **(b)**

Figure 22. Examples of beam distortions seen during the NUWC field test demonstrating (a) beam shifting, likely due to motion of the truss, and (b) beam obstruction due to macroscopic sea life; example appears to be a young jelly fish. Beam drift (a) was worse during low tide (truss closer to surface), while most of the obstructions (b) wandered into and out of the beam on the order of seconds.

4.2.2 Manual Beam Acquisition via Focal-Plane Imager

The focal-plane imager was valuable for aligning the transmit laser beam with the receive detectors. Prior to deployment, the receiver optical system was aligned so that the iris, both detectors, and the pupil-plane imager were coboresighted. The focal plane pixel representing this alignment was recorded as the target angle of arrival. After deployment in the water, the transmit beam was manually steered to maximize the coupling to the receiver detectors. Figure 23 illustrates this manual acquisition procedure carried out in the water.

While the truss held the transmitter and receiver containers relatively rigid, a manual realignment was necessary each time the truss was deployed into the water. Figure 23(a) illustrates the focal-plane response for a misalignment greater than one degree, a typical result upon deployment. The light received in the aperture is scattered from the main beam, thus the response is faint. To be observed, the focal-plane imager is set for a long exposure. The transmitter mirror is manually adjusted to steer light directly into the receive aperture; images (b) through (e) observe the focal-plane response. Once the beam is aligned, the focal-plane is saturated, so the exposure time is significantly reduced, leading to image (f). The transmit mirror is then fine tuned to steer the beam onto the target pixel. Next, the receive mirror is adjusted to optimize the angular alignment of the beam to the pupil-plane camera's and the detectors' boresight position. Boresight is verified by maintaining signal on the pupil-plane imager as the iris restricts the field of view. Manual beam alignment was accomplished typically in approximately one minute.

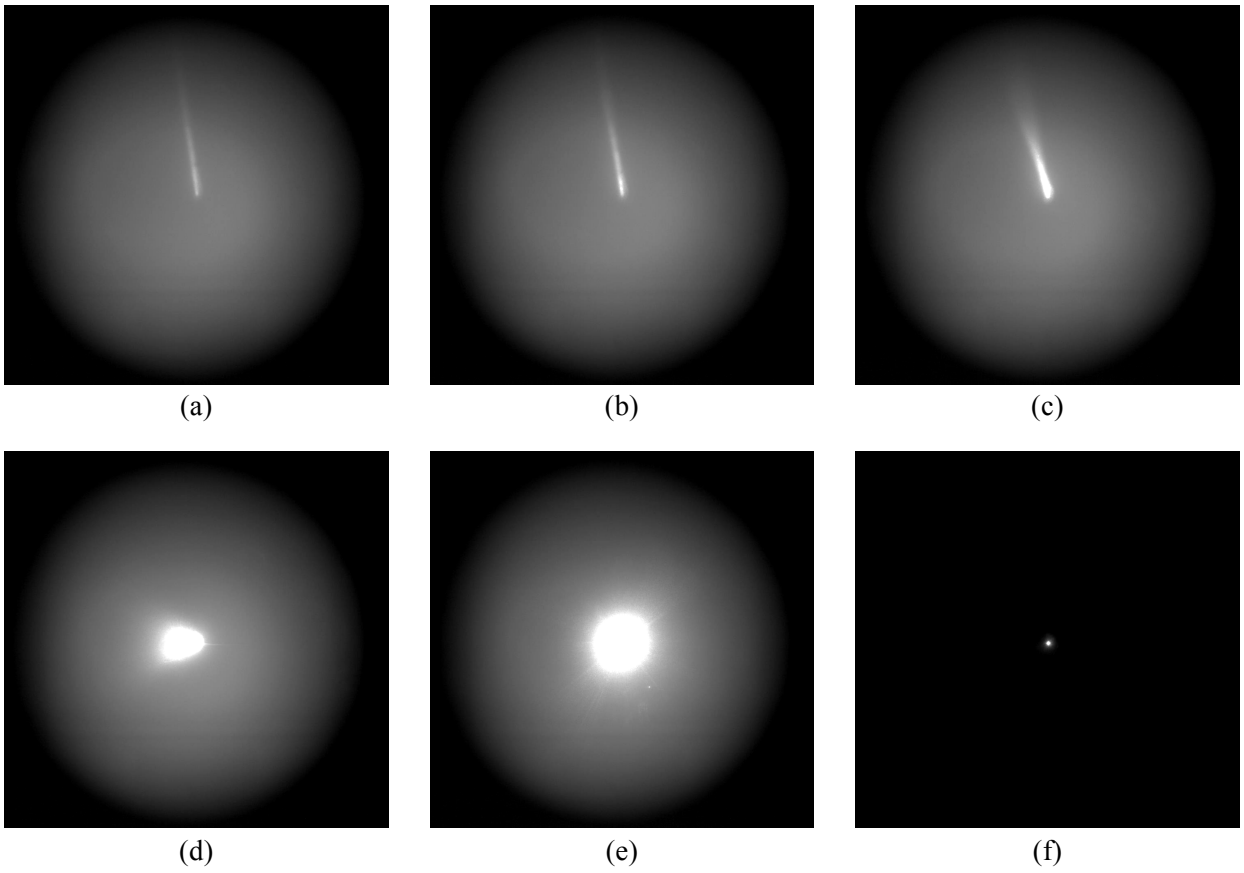

Figure 23. Focal plane images illustrating the manual alignment of the transmit beam into the receiver. Beginning with a misalignment greater than a degree in (a), the transmit beam is manually steered into alignment proceeding through (b) to (e). The camera gain is then reduced, showing the beam in a single central pixel in (f).

4.3 COMMUNICATIONS RESULTS

4.3.1 PMT Link – Performance Models and Laboratory Verification

Prior to the field test at NUWC, the PMT link was demonstrated experimentally at MIT Lincoln Laboratory. These tests (referenced below as "lab") provided verification of the receiver design and a baseline against which measurements taken at NUWC could be compared. The lab and NUWC test systems shared the same transmitter laser and transmitter driver electronics. However, each had its own PMT (both PMTs instances of the Hamamatsu H10682-210). The lab system consisted of an opaque enclosed water pipe filled with standing tap water.

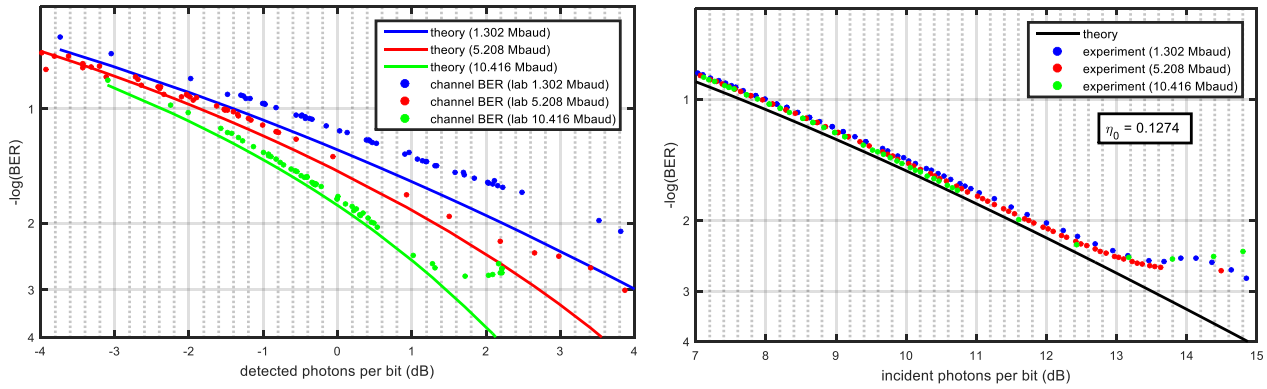

(a) (b)

Figure 24. Channel BER of laboratory system with respect to a) detected photons per bit and b) incident photons per bit. Quantum efficiency $\eta_0 = 0.1274$. Theory curves neglect background light.

Figure 24 shows the laboratory performance for the three channel rates. In all cases, the theory curves refer to the expected BER neglecting background light. In Figure 24 (a), BER is measured with respect to detected photons per bit. Figure 24 (b) shows BER with respect to incident photons per bit. It is evident from the two plots that blocking time significantly distorts the channel BER with respect to input power, and that this distortion is a function of the channel rate. On the other hand, channel BER vs. incident photons per bit follows a single theory curve, independent of channel rate. Therefore, we opt to present all subsequent results as a function of incident photons per bit.

The performance of the FEC decoder was also demonstrated at all channel rates. At each channel rate, three code rates (1/2, 2/3, and 5/6) were tested. Figure 25 shows the receiver performance over all channel and code rates. Figure 25 also shows the distance to capacity at each code rate. This distance was 1.6 to 2.1 dB at all rates.

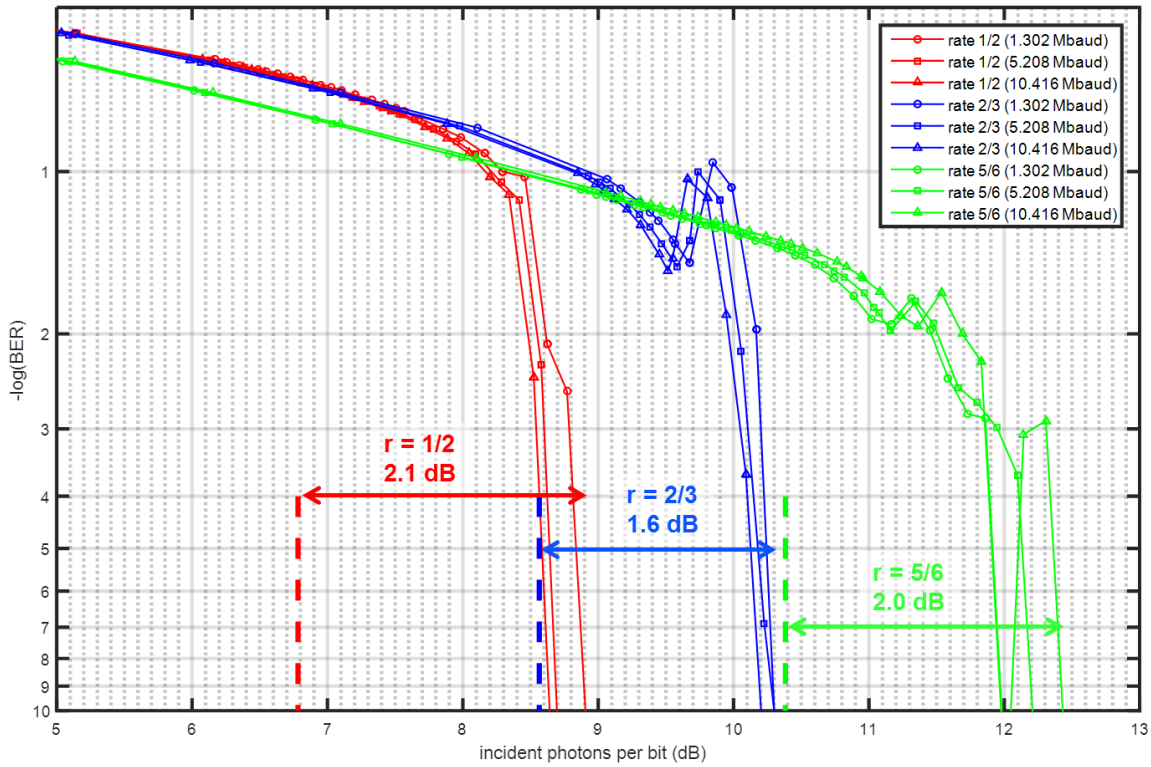

Figure 25. Lab performance of FEC decoder over all channel and code rates and distance to capacity (dashed vertical lines) at each code rate.

4.3.2 PMT Link – NUWC Field Test Results

"First Light" Measurement The field system was lowered into the water during the afternoon on 29 March 2016. After manual alignment, an initial communication measurement was started at 5:25 PM. During this time, the sky was clear and sunny. To mitigate background light, the iris opening was set to a field of view of 5.5 mrad (full angle). Figure 26 shows the measured channel and post-FEC BER for the "first light" demonstration. Each data point corresponds to a measurement integrated over at least 10 seconds. Error-free performance was achieved at a sensitivity of 11.3 dB incident photons per bit.

During the first light measurement, the received signal exhibited minor beam wander in the pupil-plane image, most likely due to wave-induced truss motion. Occasionally, the wander resulted in momentary signal loss due to the iris constriction. The channel BER was observed to be slightly degraded compared to laboratory performance. The in-harbor result was 0.4 dB from the theoretical (no background) result. Thus, the natural water conditions, including beam wander, caused only an additional 0.2 dB penalty over what was observed in the laboratory.

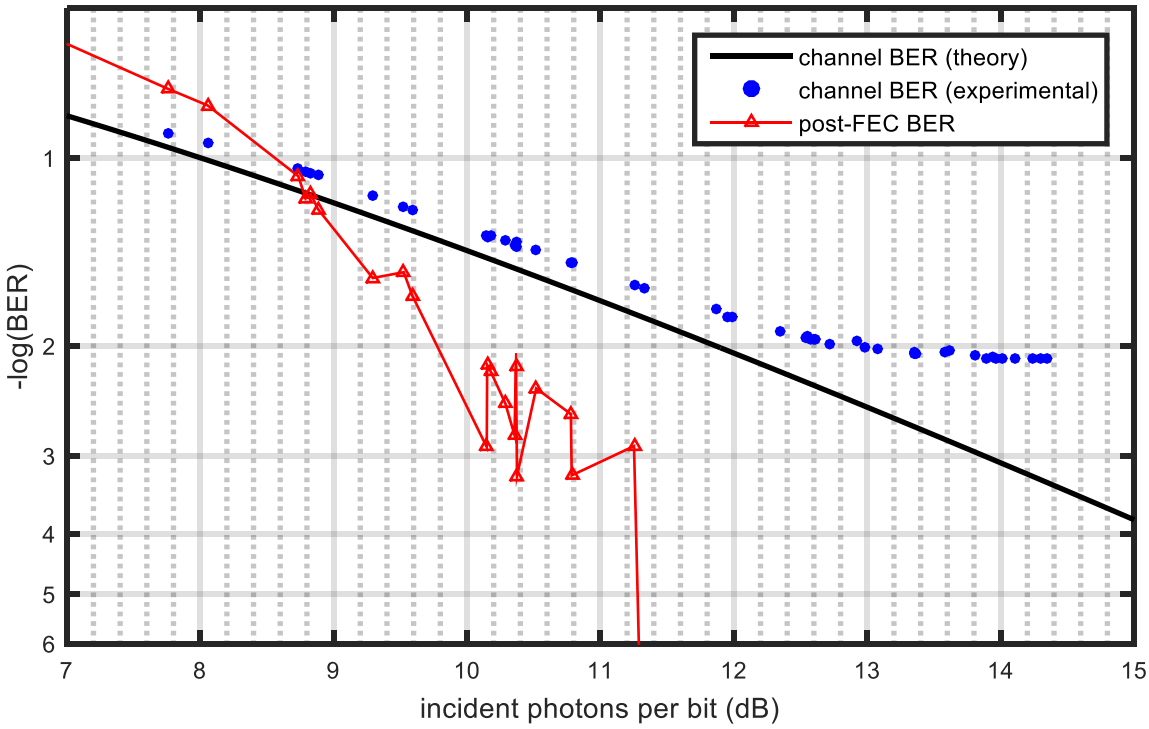

Figure 26. Daylight BER measurement at 10.416 Mbaud and code rate = 1/2 on 29 March 2016. Iris opening diameter is 0.275 mm and field of view is 5.5 mrad.

Nighttime PMT Measurements Additional measurements were taken after sunset on 29 March, starting at 8:50 PM. These measurements consisted of link measurements at each of the channel rates (10.4, 5.2, or 1.3 Mbaud) while the decoder was configured for code rate = 1/2. For these tests, the dock lights were shut off to minimize ambient light. Furthermore, the iris was opened to a field of view of 8.9 mrad.

Figure 27 shows the channel BER and the post-FEC BER at all three channel rates. Error-free performance was achieved; however, compared to the laboratory measurements, the performance was much noisier in the region where it should be error free. We ascribe this behavior to beam wander due to flexing of the metal framework of the communication apparatus combined with the receiver's small field of view. The weather was windy with significant wave motion. We believe that the fluctuations seen in the post-FEC BER are due to the beam wandering in and out of the field of view. Nevertheless, the onset of error-free performance occurs at 8.8 dB incident signal photons per bit, which is very close to the behavior seen in the laboratory. Given the field of view, it is likely that the beam motion resulted in power fluctuations at the PMT that did not significantly affect the channel BER measurement but did cause the decoder to fail on occasion. We expect that with closed-loop beam tracking, these fluctuations can be largely mitigated.

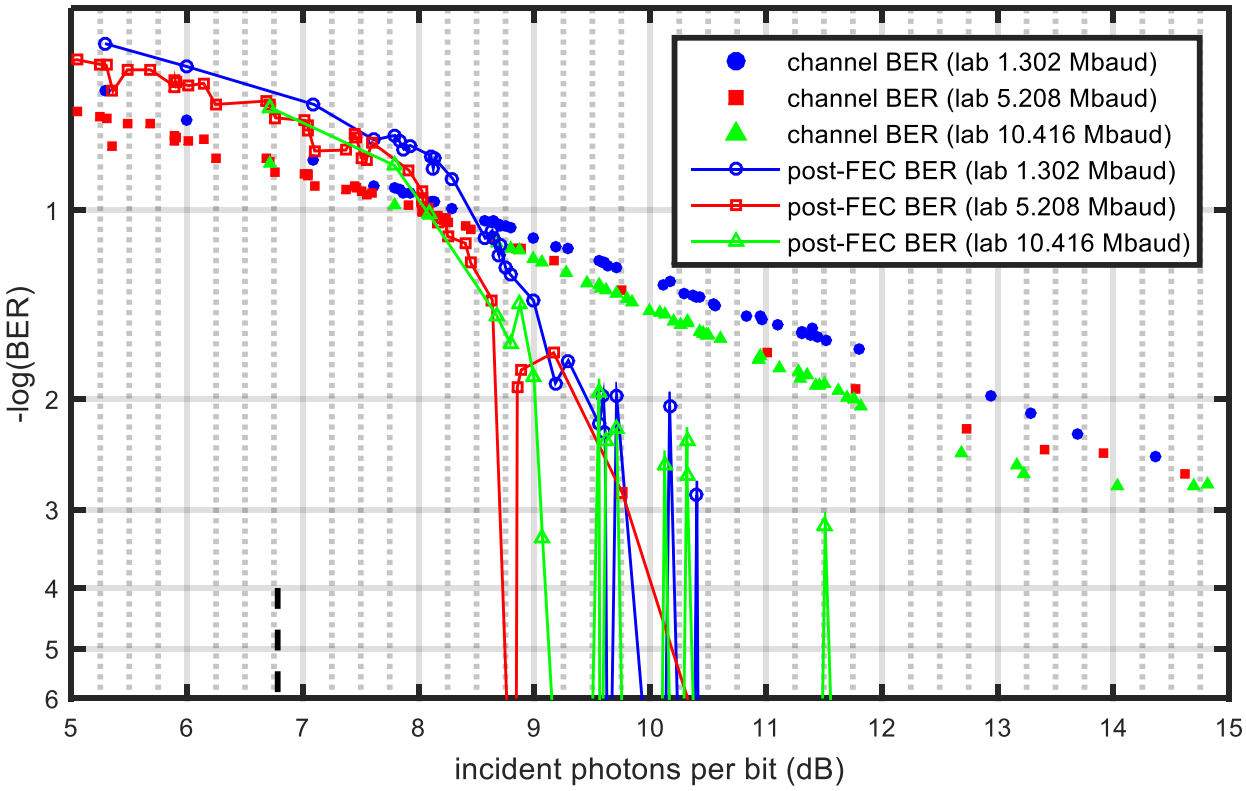

Figure 27. FEC performance (code rate = 1/2) for nighttime measurements of all channel rates on 29 March 2016.

Daytime PMT Measurement with Code Rate 5/6 A daylight measurement at 10.416 Mbaud and code rate = 5/6 was performed. This represents the maximum data rate of the PMT transceiver. The field of view was set to 3.8 mrad to minimize background light. The results are shown in Figure 28. For the channel BER, an approximately 0.3 dB penalty was observed, a penalty of 0.1 dB compared to night operation. Error-free operation was achieved for approximately 12.5 dB photons per bit, similar to laboratory measurements. The post-FEC transition to error-free performance was cleaner than during the night experiment. The weather and waves were much calmer, which likely reduced truss flexing and therefore decreased the beam wander. Compared to the laboratory experiment in Figure 25, the onset of error-free performance at this code rate occurs at approximately 0.4 dB higher input power. Daylight operation results in only a very small and manageable penalty compared to a controlled laboratory experiment.

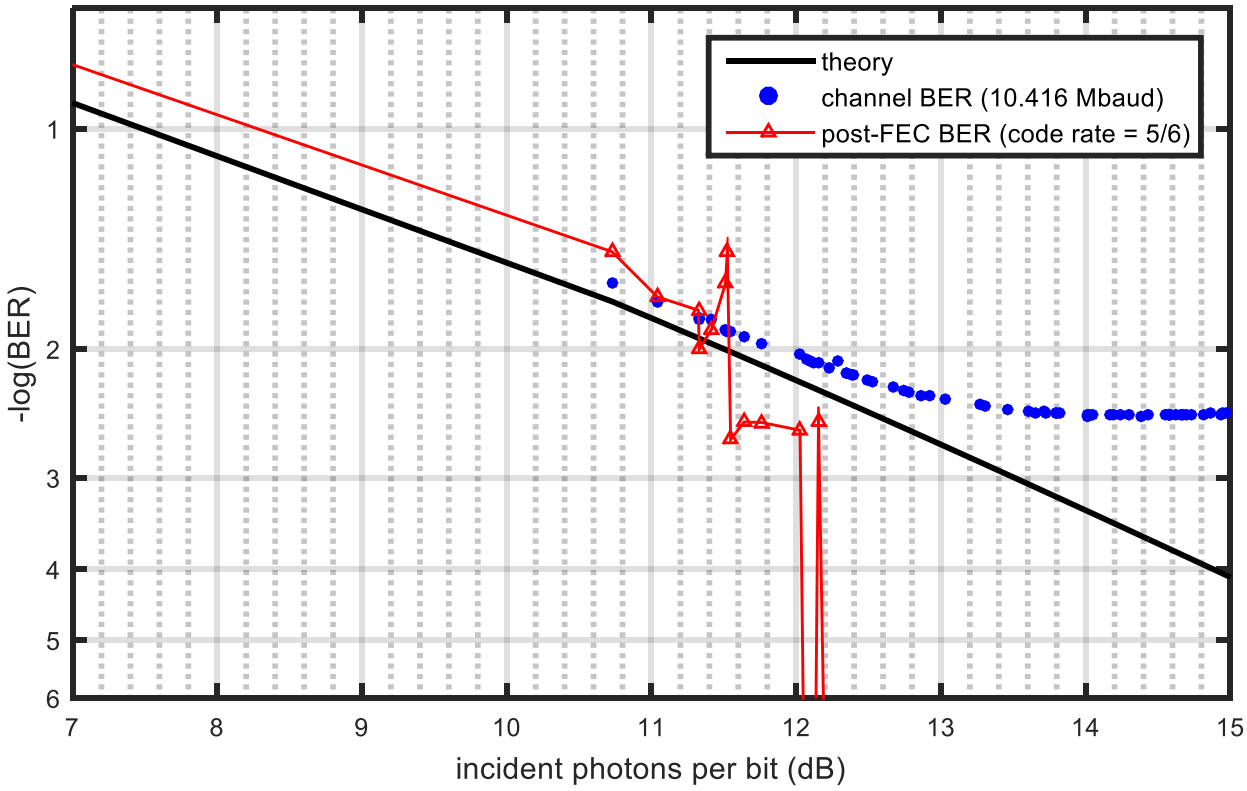

Figure 28. Daylight BER measurement at 10.416 Mbaud and code rate = 5/6 on 30 March 2016.

Narrow vs. Wide Field of View Daytime measurements were taken with fields of view of 5.5 mrad and 158.5 mrad to determine the penalty for a wider view. The channel rate was 1.3 Mbaud and the code rate was 1/2. The weather conditions were bright and calm. Figure 29 shows the results. Both links achieved error-free performance, but the wider field of view resulted in a relative power penalty of 8.3 dB. Nevertheless, this experiment demonstrated that the photon-counting receiver could tolerate high background levels; in fact, in this case, error-free performance could be achieved when the signal power was 0.7 dB below the background power.

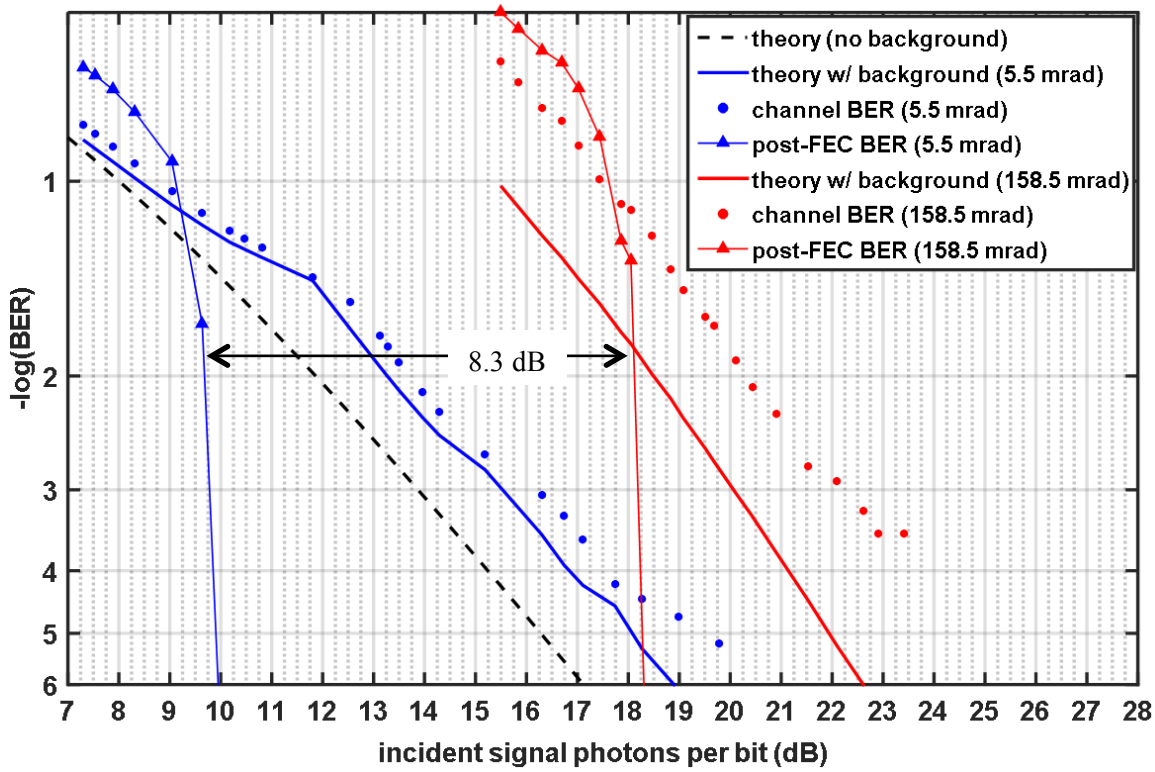

Figure 29. Pre-FEC channel BER and post-FEC performance of 1.3 Mbaud PMT link in daylight with narrow (5.5 mrad) and wide (158.5 mrad) fields of view.

4.3.3 APD Link

Initial testing of the 125 Mb/s link was performed over a range of 4.8 meters (15.75 ft) in 9 feet of water at the maximum transmitter power (achieved by removing the VOA from the transmitter). The extinction coefficient was measured to be 1 m^{-1} by the LISST-100X during this time implying a link range of 4.8 extinction lengths. The transmitted data was repetitions of a pseudorandom binary sequence consisting of 127 bits. During this test two bit errors occurred during a 60 second observation indicating an error rate less than 10^{-9}.

Subsequent testing was performed at lower power levels by reinserting the VOA into the transmitter fiber. In this configuration, the received waveform was captured on an oscilloscope and post-processed for a range of transmitter powers. Two daytime measurements were taken of the APD link at high rate and high SNR. The channel BER for each field test and laboratory results are shown in Figure 30. Good agreement was obtained between laboratory and field data at low powers. In particular, the field data matched the behavior of the laboratory data in the region where FEC performance transitions to error free (28 dB signal photons per bit, or –45.2 dBm). At higher powers, the field data deviated significantly from

the data obtained in the laboratory. This departure was likely caused by the VOA; without the VOA, the channel BER dropped to better than 10^{-9}.

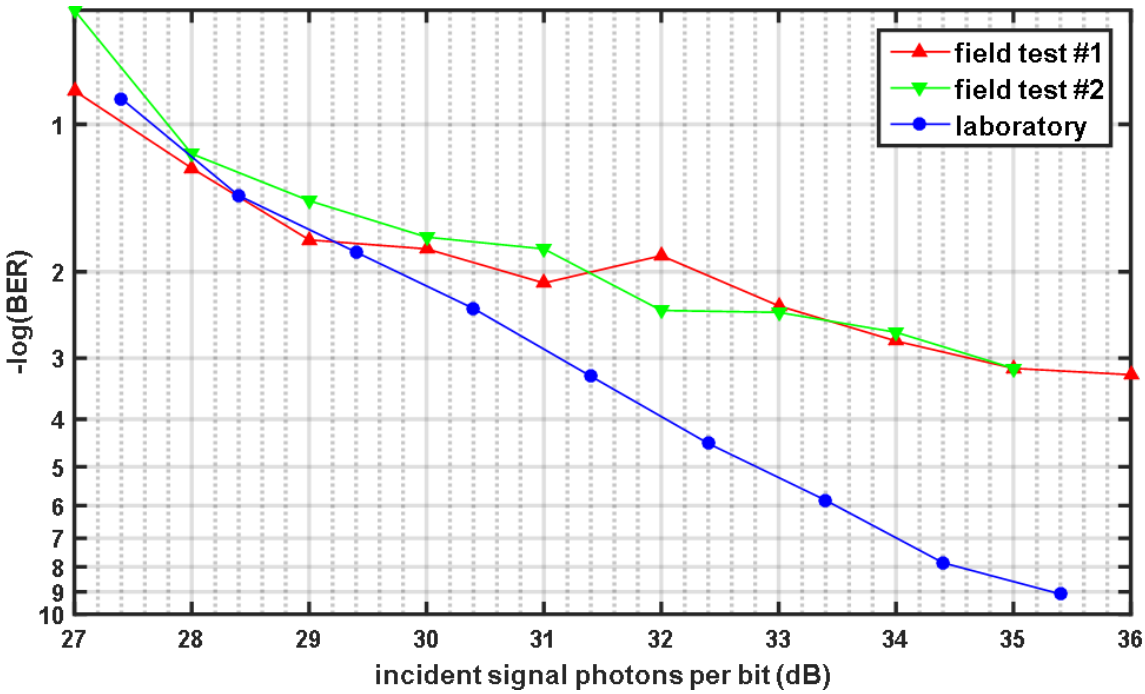

Figure 30. The BER versus transmitter attenuation for a 125 Mb/s NRZ-OOK link through 4.8 meters of harbor water. The circle and cross markers indicate data from two measurement taken approximately 30 minutes apart.

4.3.4 Summary of Communication Results

Table 7 summarizes the communications experiments conducted for with the PMT and APD detectors, including the tide, the wind speed, the estimate for the attenuation coefficient *c* at the time of the demo, and the length of the link (in meters and extinction length).

TABLE 7

Summary of Communications Results

Date/Time	Conditions		Baud Rate/ Data Rate	Field of View (mrad)	c (m^{-1})	Link Distance
	Tide	Wind (km/h)				
3/29/16 5:30 PM	Low	32	10.4 Mbaud 5.2 Mbps	5.5	1.43	7.8 m 11.2 L_{ext}
3/29/16 8:49 PM	Flood (L+3)	24	10.4 Mbaud 5.2 Mbps	8.9	1.11	7.8 m 8.7 L_{ext}
3/29/16 10:19 PM	Flood (H-2)	24	5.2 Mbaud 2.6 Mbps	8.9	1.18	7.8 m 9.2 L_{ext}
3/29/16 11:08 PM	Flood (H-1)	24	1.3 Mbaud 0.65 Mbps	8.9	1.16	7.8 m 9.0 L_{ext}
3/30/16 11:56 AM	Flood (H-1)	11	10.4 Mbaud 8.7 Mbps	3.8	1.01	7.8 m 7.9 L_{ext}
3/30/16 1:27 PM	High	24	1.3 Mbaud 0.65 Mbps	160	1.06	7.8 m 8.3 L_{ext}
3/30/16 1:44 PM	High	24	1.3 Mbaud 0.65 Mbps	5.5	1.07	7.8 m 8.3 L_{ext}
3/30/16 3:32 PM	Ebb (H+2)	16	10.4 Mbaud 5.2 Mbps	5.5	1.17	7.8 m 9.1 L_{ext}
3/30/16 3:43 PM	Ebb (H+2)	16	10.4 Mbaud 5.2 Mbps	14	1.17	7.8 m 9.1 L_{ext}
3/30/16 3:51 PM	Ebb (H+2)	21	10.4 Mbaud 5.2 Mbps	22.5	1.17	7.8 m 9.1 L_{ext}
3/30/16 4:02 PM	Ebb (H+2)	21	10.4 Mbaud 5.2 Mbps	31	1.21	7.8 m 9.4 L_{ext}
3/30/16 4:09 PM	Ebb (H+2)	21	10.4 Mbaud 5.2 Mbps	39.5	1.18	7.8 m 9.2 L_{ext}
3/30/16 6:14 PM	Low	16	5.2 Mbaud 2.6 Mbps	22.5	1.52	7.8 m 11.9 L_{ext}
3/30/16 7:47 PM	Flood (L+1)	13	10.4 Mbaud 5.2 Mbps	160	1.50	7.8 m 11.7 L_{ext}
3/30/16 8:03 PM	Flood (L+2)	13	5.2 Mbaud 2.6 Mbps	160	1.46	7.8 m 11.3 L_{ext}
3/30/16 8:18 PM	Flood (L+2)	13	1.3 Mbaud 0.65 Mbps	160	1.33	7.8 m 10.4 L_{ext}
3/30/16 8:32 PM	Flood (L+2)	13	10.4 Mbaud 5.2 Mbps	160	1.35	7.8 m 10.5 L_{ext}
3/31/16 10:30 AM	Flood (L+3)	24	125 Mbaud 125 Mbps	12.5	1.07	4.8 m 5.1 L_{ext}
3/31/16 11:00 AM	Flood (L+3)	24	125 Mbaud 125 Mbps	12.5	1.10	4.8 m 5.3 L_{ext}
3/31/16 1:30 PM	High	21	125 Mbaud 125 Mbps	12.5	0.93	4.8 m 4.5 L_{ext}

This page intentionally left blank.

5. CONCLUSION

The undersea lasercom field test was a proof of concept pathfinder toward a narrow-beam undersea prototype. The field test met its objectives by demonstrating real-time laser communication and characterizing laser beam propagation through natural waters. Principal accomplishments include:

- Demonstration of a real-time, single-photon sensitive, communication undersea lasercom with data rates between 0.65 and 8.7 Mbps over a distance of 7.8 m, corresponding to 8–12 extinction lengths;
- Demonstration of robust communication during both day and night background light levels;
- Demonstration of a real-time communication undersea lasercom with a data rate of 125 Mbps over a distance of 4.8 m, corresponding to 5 extinction lengths;
- Stable alignment of a collimated laser beam through harbor waters between two fixed terminals;
- Development of a burst-mode lasercom transceiver with real-time FPGA electronics supporting a commercial PMT detector; and
- Characterization data to validate modeled lasercom performance predictions.

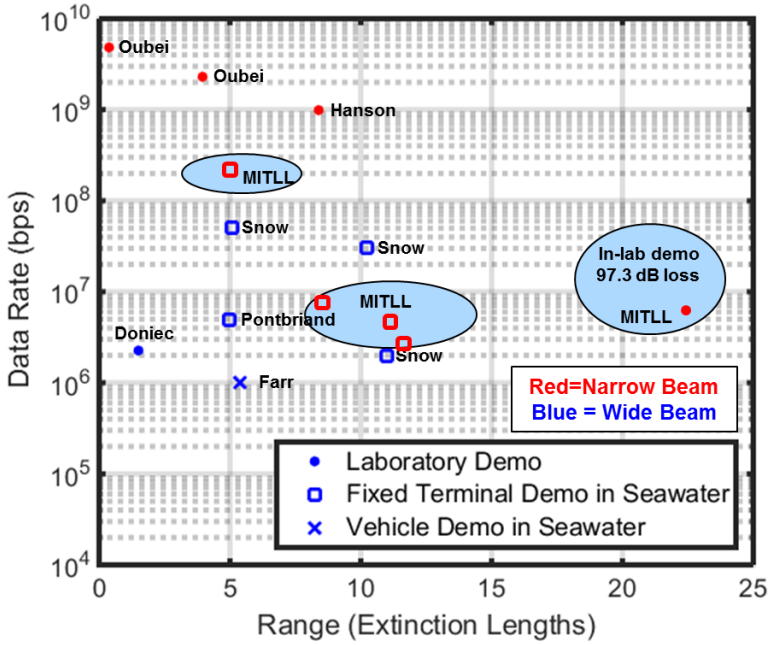

Figure 31. Comparison of MIT Lincoln Laboratory communications field results to published demonstrations. Note that the achieved performance was accomplished despite using only 0.25 mW of transmitted optical power and most of the received light being coupled to the imaging cameras (i.e., not used in the communication demonstration).

Figure 31 compares the demonstrations from the MIT Lincoln Laboratory field demonstration with the selected published demonstrations from Figure 1. The PMT links achieved a longer range in extinction lengths than previous in-water communications demonstrations. The APD link closed 5 extinction lengths at 125 Mbps, representing the highest-rate published in-water demonstration. We note that the field test results are achieved despite experimental constraints that "artificially" increased the loss. Specifically, the inclusion of the VOA, transmit fiber from the on-shore laser to the transmit container, and receive beamsplitters to share the light between two cameras and two communications detectors added 25–30 dB of loss. When designing a prototype lasercom terminal, such losses would be minimized or eliminated altogether. It is worth noting that the in-lab demonstration of the PMT transceiver achieved error-free performance at 5.2 Mbps with 97.3 dB of attenuation; this corresponds to 22 extinction lengths of attenuation. This would correspond to between 15 and 23 meters of harbor water as seen during the field test. Translating this performance to a clear ocean and blue wavelength scenario suggests links in excess of 400 meters are achievable with small, low-power, narrow-beam lasercom terminals.

The field test proved the feasibility of narrow-beam communication through natural waters and provided valuable data for the design of a prototype undersea lasercom terminal.

REFERENCES

1 J.B. Snow, J.P. Flatley and D.E. Freeman, “Underwater propagation of high-data-rate laser communications pulses, ” *Proc. SPIE,* Vols. 1750, 1992, pp. 419–427.

2 C. Pontbriand, N. Farr, J. Ware, J. Preisig and H. Popenoe, “Diffuse high-bandwidth optical communications, ” in OCEANS 2008.

3 N. Farr, J. Ware, C. Pontbriand, T. Hammar and M. Tivey, “Optical communication system expands CORK seafloor observatory’s bandwidth, ” in OCEANS 2010.

4 F. Hanson and S. Radic, “High bandwidth underwater optical communication, ” *Applied Optics*, Vols. 47, 2008, pp. 277–283.

5 H.M. Oubei, J.R. Duran, B. Janjua, H.-Y. Wang, C.-T. Tsai, Y.-C. Chi, T.K. Ng, H.-C. Kuo, J.-H. He, M.-S. Alouini, G.-R. Lin and B.S. Ooi, “4.8 Gbit/s 16-QAM-OFDM transmission based on compact 450-nm laser for underwater wireless optical communication, ” *Opt. Express*, vol. 23, pp. 23302–23309, 2015.

6 H.M. Oubei, C. Li, K.-H. Park, T.K. Ng, M.-S. Alouini and B.S. Ooi, “2.3 Gbit/s underwater wireless optical communications using directly modulated 520 nm laser diode, ” *Optics Express*, vol. 23, no. 16, pp. 20743–20748, 2015.

7 M. Doniec and D. Rus, “Bidirectional optical communication with AquaOptical II, ” in Communication Systems (ICCS), 2010 IEEE International Conference on, Singapore, 2010.

This page intentionally left blank.

REPORT DOCUMENTATION PAGE

Form Approved
OMB No. 0704-0188

1. REPORT DATE *(DD-MM-YYYY)*	**2. REPORT TYPE**	**3. DATES COVERED** *(From - To)*
08-30-2016	Technical Report	

4. TITLE AND SUBTITLE

Undersea Laser Communications Field Test at the Naval Undersea Warfare Center (NUWC)

5a. CONTRACT NUMBER
FA8721-05-C-0002 & FA8702-15-D-0001

5b. GRANT NUMBER

5c. PROGRAM ELEMENT NUMBER

6. AUTHOR(S)

Andrew S. Fletcher, Hemonth G. Rao, Nicholas D. Hardy, Catherine E. DeVoe, Igor D.Gaschits, Farhad Hakimi, Scott A. Hamilton, John G. Ingwersen, Richard D. Kaminsky, Marvin S. Scheinbart, and Timothy M. Yarnall

5d. PROJECT NUMBER
2238

5e. TASK NUMBER

5f. WORK UNIT NUMBER

7. PERFORMING ORGANIZATION NAME(S) AND ADDRESS(ES)

MIT Lincoln Laboratory
244 Wood Street
Lexington, MA 02420-9108

8. PERFORMING ORGANIZATION REPORT NUMBER

TR-1213

9. SPONSORING / MONITORING AGENCY NAME(S) AND ADDRESS(ES)

Office of the Assistant Secretary of Defense, Research and Engineering
3040 Defense Pentagon
Room 3C855A
Washington, DC 20301

10. SPONSOR/MONITOR'S ACRONYM(S)
ASD(R&E)

11. SPONSOR/MONITOR'S REPORT NUMBER(S)

12. DISTRIBUTION / AVAILABILITY STATEMENT

Approved for public release: distribution unlimited.

13. SUPPLEMENTARY NOTES

14. ABSTRACT

Narrow-beam laser communication (lasercom) has the potential to maximize both the achievable range and data rate of undersea optical communications. MIT Lincoln Laboratory conducted a field demonstration of narrow-beam undersea lasercom from 28 March–1 April 2016 at the Naval Undersea Warfare Center (NUWC) in Middletown, RI. Transmit and receive hardware were placed in two watertight containers and attached to the ends of an aluminum truss which was lowered alongside a pier into the Narragansett Bay. A green (515 nm wavelength) collimated laser beam was modulated and steered into a receiver with four sensors: two cameras to provide alignment and beam characterization data and two photodetectors to provide distinct high-speed communications demonstrations. The first demonstration utilized a single-photon sensitive photomultiplier tube (PMT) and achieved data rates up to 8.7 megabits per second (Mbps) over a distance of 7.6 meters, which corresponded to between 8–12 beam extinction lengths. The PMT demonstration included real-time electronics to perform synchronization and forward error correction and achieved a sensitivity of better than 1.5 detected photons per bit. In the second demonstration, a 125 Mbps communications link was demonstrated over 4.8 meters (5 beam extinction lengths) with an avalanche photodiode (APD) receiver. Communications and characterization data were collected through a variety of conditions over the five-day field experiment, including day and night, calm and high winds, and flood and ebb tide; robust communication performance was achieved throughout. In the experiment the transmit power, receiver field of view, and link distance were varied. The water transmissivity and volume scattering function were measured throughout the experiment to calibrate the results. The field test data for both communication and beam propagation characterization provide in-water validation of model-generated lasercom performance predictions.

15. SUBJECT TERMS

16. SECURITY CLASSIFICATION OF:			**17. LIMITATION OF ABSTRACT**	**18. NUMBER OF PAGES**	**19a. NAME OF RESPONSIBLE PERSON**
a. REPORT	**b. ABSTRACT**	**c. THIS PAGE**			**19b. TELEPHONE NUMBER** *(include area code)*
Unclassified	Unclassified	Unclassified	Same as report	56	

This page intentionally left blank.